



The dynamics of Kerguelen Plateau magma evolution: New insights from major element, trace element and Sr isotope microanalysis of plagioclase hosted in Elan Bank basalts

William S. Kinman^{a,c,*}, Clive R. Neal^a, Jon P. Davidson^b, Laura Font^{b,d}

^a Department of Civil Engineering and Geological Sciences, University of Notre Dame, 156 Fitzpatrick Hall, Notre Dame, IN 46556, United States

^b Department of Earth Sciences, University of Durham, Durham DH1 3LE, UK

^c Chemistry Division, Nuclear and Radiochemistry, Los Alamos National Laboratory, MSJ514, Los Alamos, NM 87545, United States

^d IVA – Earth Sciences – Petrology Department, Vrije Universiteit Amsterdam, De Boelelaan 1085, Amsterdam, Netherlands

ARTICLE INFO

Article history:

Received 26 June 2008

Received in revised form 18 February 2009

Accepted 9 March 2009

Editor: D.B. Dingwell

Keywords:

Kerguelen

Laser ablation

Microanalysis

Large igneous province

Ocean Drilling Program

ABSTRACT

The Kerguelen Plateau and Broken Ridge in the southern Indian Ocean together represent one of the most voluminous large igneous provinces (LIPs) ever emplaced on Earth. A scientific objective of Ocean Drilling Program (ODP) Leg 183 was to constrain the post-melting magma evolution of Kerguelen Plateau magmas. In an effort to better understand this evolution, isotopic and trace element analysis of individual plagioclase crystals hosted within two Kerguelen Plateau basalts recovered from Elan Bank were undertaken. Previous whole-rock studies established that the two host basalts investigated in this study are samples of crustally contaminated (lower group) and relatively uncontaminated (upper group) basalt.

Plagioclase phenocrysts from the uncontaminated basalt are dominantly normal zoned and exhibit a $^{87}\text{Sr}/^{86}\text{Sr}_i$ range of 0.704845–0.704985, which overlaps uncontaminated group whole-rock values previously reported. Plagioclase crystals from the contaminated basalt are dominantly reverse zoned and exhibit a $^{87}\text{Sr}/^{86}\text{Sr}_i$ range of 0.705510–0.705735, which all lie within contaminated group whole-rock values previously reported. There are no systematic within crystal core to rim variations in $^{87}\text{Sr}/^{86}\text{Sr}_i$ from either group, with the exception that contaminated group crystal rims have overall less radiogenic $^{87}\text{Sr}/^{86}\text{Sr}_i$ than other zones. These observations indicate that crustal assimilation occurred before the formation of Unit 10 plagioclase phenocrysts, which is supported by parent magma trace element abundance data inverted using carefully calculated partition coefficients. Trace element diffusion modeling indicates that the upper group basalt (Unit 4) experienced a more vigorous eruptive flux than the lower group basalt (Unit 10).

We suggest that plagioclase phenocrysts in both the upper and lower group basalts originated from the shallowest section of what was likely a complex magma chamber system. We contend that the magmatic system contained regions of extensive plagioclase-dominated crystal mush. Crustal assimilation was not a significant ongoing process in this portion of the Elan Bank magmatic system. Both basalts exhibit compelling evidence for remobilization and partial resorption of crystalline debris (e.g., reverse zoned crystals, glomerocrysts). We suggest Unit 4 and 10 magmas ascended different sections of the Elan Bank magma system, where the Unit 10 magmas ascended a section of the magma system that penetrated a stranded fragment of continental crust.

© 2009 Elsevier B.V. All rights reserved.

1. Introduction

Large igneous provinces (LIPs) are voluminous emplacements of basaltic magma formed over geologically short spans of time (Coffin and Eldholm, 1994; Duncan, 2002). The submarine Kerguelen Plateau (KP) and Broken Ridge rise up to 4 km above the surrounding Indian Ocean basin and constitute the second largest oceanic LIP on Earth (Fig. 1). Studies of LIPs such as the expansive KP are important for

several reasons including: 1) LIPs sample portions of the mantle not thought to be tapped during normal mid-ocean ridge spreading and help us better understand the broader mantle composition, 2) Cretaceous LIP volcanism represented as much as 50% of the global volcanic output, whereas LIPs currently represent <10% of the output signifying large scale changes in mantle dynamics, and 3) rapid formation of LIPs such as the KP may have had catastrophic effects on the environment (Coffin and Eldholm, 1994; Shipboard Scientific Party, 2000). Oceanic LIPs such as the KP are among the least understood geologic features on the planet. This is due in part to the practical difficulties of sampling these largely submerged oceanic plateaus. Current sampling of the Cretaceous portion of the KP has been

* Corresponding author. Chemistry Division, Nuclear and Radiochemistry, Los Alamos National Laboratory, MSJ514, Los Alamos, NM 87545, United States, Tel.: +505 667 5910.

E-mail address: wkinman@lanl.gov (W.S. Kinman).

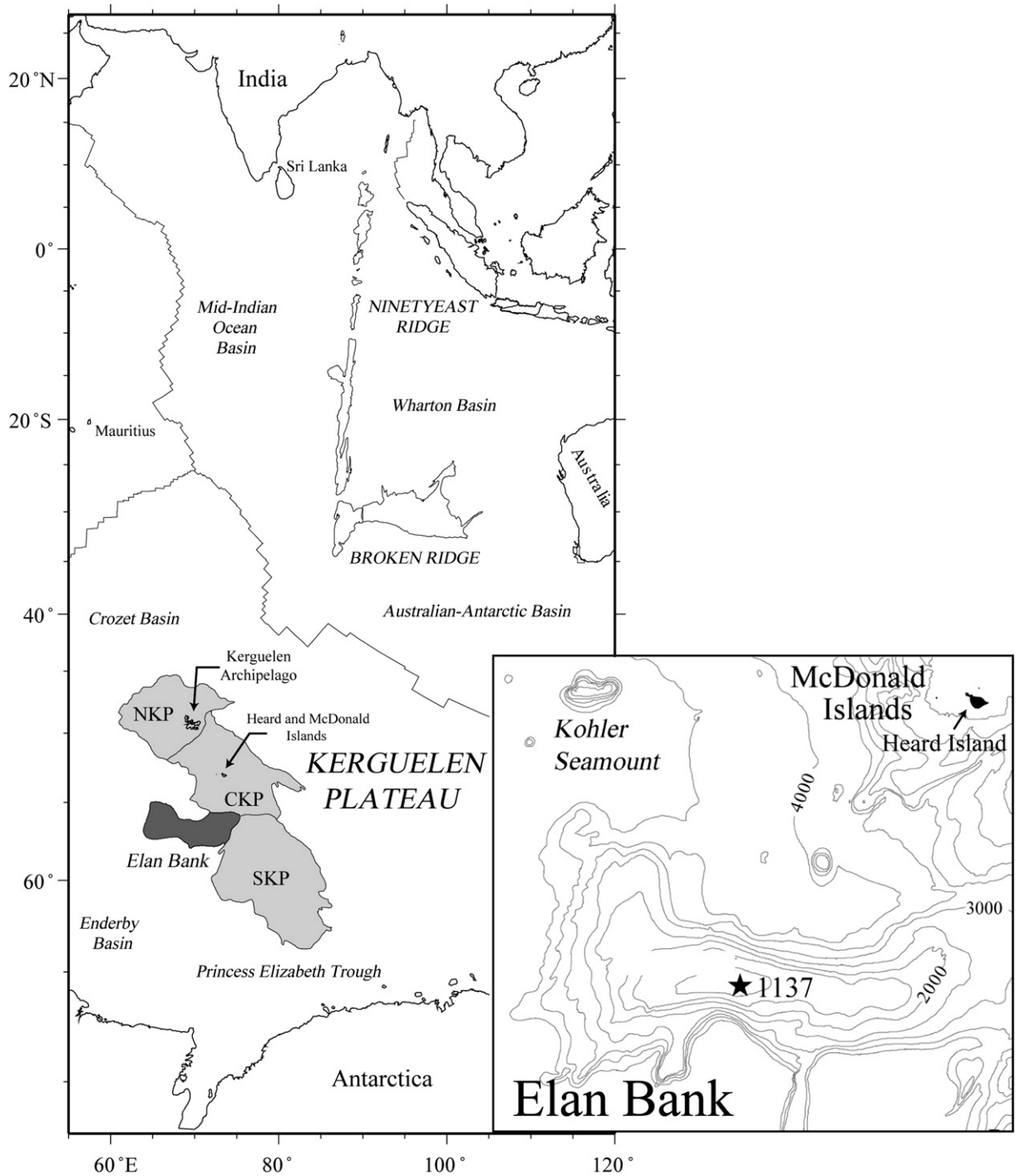


Fig. 1. Map of the Indian Ocean showing the Kerguelen Plateau (KP) and other features attributed to the Kerguelen plume. Inset bathymetric map of Elan Bank and the location of ODP Site 1137. NKP is Northern KP, CKP is the Central KP, and SKP is the Southern KP. Maps adapted from Shipboard Scientific Party (2000).

achieved via drilling at 11 drill sites during Ocean Drilling Program Legs 119, 120, and 183.

Prior to ODP Leg 183 a number of researchers suggested that continental crust was involved during the petrogenesis of some KP basalts (e.g., Frey et al., 2002; Mahoney et al., 1995). Drilling at Site 1137 on Elan Bank confirmed hypotheses of crustal involvement when clasts of garnet–biotite gneiss were recovered from an interflow fluvial conglomerate unit (Unit 6 in Fig. 2) (Shipboard Scientific Party, 2000; Ingle et al., 2002a). Nicolaysen et al. (2001) and Frey et al. (2000) suggested that during the break up of the Gondwana

supercontinent fragments of old continental crust were stranded among the Indian Ocean lithosphere. One of the scientific objectives of Leg 183 drilling was to constrain the post-melting evolution of Kerguelen magmas. This investigation explores the isotopic and trace element record of KP magma evolution preserved within zoned plagioclase phenocrysts hosted in two KP basalts. Based upon previous work, the consensus view is that one of the basalts selected for this study is crustally contaminated (ODP Leg 183 Site 1137 Unit 10), whereas the other is not (Site 1137 Unit 4) (Ingle et al., 2002b). Examination of plagioclase phenocrysts from relatively contaminated

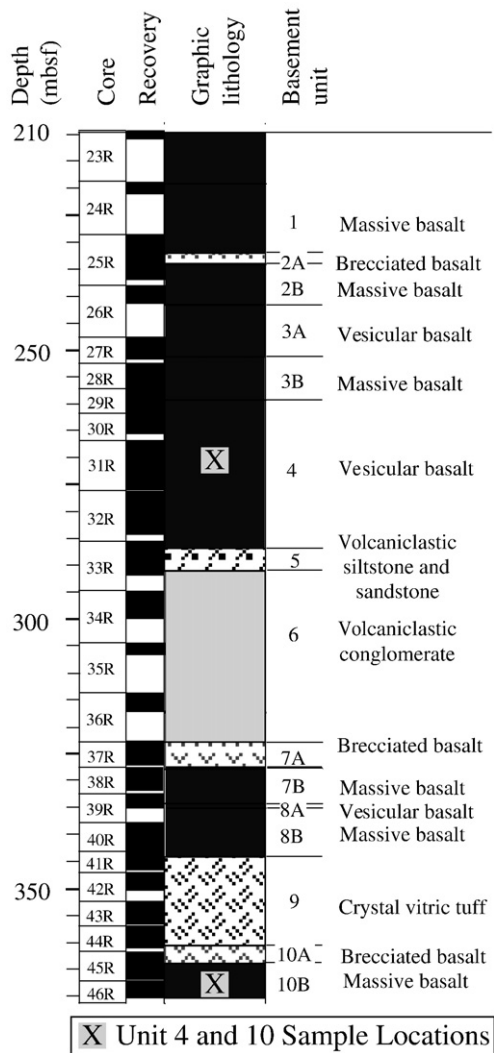


Fig. 2. The cored section of igneous rocks from ODP Site 1137. The locations of each sample used in this study is shown as a boxed in X. Segments where rock was recovered during coring are shown as black in the 'recovery' column. Basement unit boundaries are designated at lava flow tops/bottoms. Figure adapted from Shipboard Scientific Party (2000).

as well as uncontaminated KP basalts provides snapshots of KP magma evolution both when an open system process (i.e., crustal assimilation) was significant and when it was not.

Strontium isotope data were collected from multiple individual plagioclase crystals using microdrilling, low-blank chemistry, and measurement by multicollector TIMS. Trace element data were collected from the same crystals using a combination of Electron Probe Microanalysis (EPMA) and Laser Ablation Inductively Coupled Plasma Mass Spectrometry (LA-ICP-MS). The trace element record within a zoned plagioclase phenocryst is best understood via reconstruction of parent magma composition using appropriate partition coefficients. The value in reconstructing the trace element composition of a mineral's parent magma in combination with Sr isotope data measured in individual zones within a crystal is that one can access the nature of batches of magma that have long since been homogenized into a larger magma system. This approach provides a picture of magma evolution not easily attained using whole-rock data alone e.g., Davidson et al. (2005).

1.1. Geologic background of the Kerguelen Plateau and Elan Bank

The bulk of the 2×10^6 km² Kerguelen Plateau formed during the Cretaceous (Coffin and Eldholm, 1994, 1993; Duncan, 2002). Formation

of the KP has been ascribed to surfacing of the Kerguelen plume and is closely spaced in time with the break up of India and Australia at ~132 Ma (Kent et al., 2001). Broken Ridge was separated from the KP during the Early Tertiary with the onset of spreading at the Southeast Indian Ridge (Neal et al., 2002) (Fig. 1). The Kerguelen Plateau has been divided into distinct sections, which include the Southern KP, Central KP, Northern KP, and Elan Bank (Frey et al., 2000) (Fig. 1). The northerly trending Ninetyeast Ridge has been attributed to Kerguelen plume tail volcanism (e.g., Saunders et al., 1991), and Heard and McDonald Islands represent the most recent volcanism ascribed to the Kerguelen plume. Elan Bank is a salient that extends from the western edge of the KP and contains a number of seismic reflections consistent with the presence of continental crust (Shipboard Scientific Party, 2000).

2. Samples

The Unit 4 basalt represents a relatively uncontaminated single 27 m thick variably vesicular subaerial plagioclase phyric inflated pahoehoe flow (Shipboard Scientific Party, 2000). A sample was selected from a portion of the Unit 4 flow that exhibited the least alteration and lowest vesicle content (183-1137A-32R-05W-22-27; Fig. 2). The Unit 10 basalt represents a crustally contaminated basalt from the bottom of the Site 1137 cored section. Unit 10 consists of the top of a subaerial massive plagioclase phyric basalt flow (Shipboard Scientific Party, 2000). A sample was selected for analysis from a minimally altered portion of the Unit 10 flow (183-1137A-46R-01W-20-35; Fig. 2).

3. Analytical techniques

Basalt samples were prepared as polished thin sections using a microdiamond slurry and final grit size of 0.5 μ m. More details on sample preparation can be found in Kinman and Neal (2006).

3.1. Electron Probe Microanalysis (EPMA) and Scanning Electron Microscopy

Backscatter electron images and major element analyses were performed using a JEOL JXA-8600 Superprobe electron microprobe at the University of Notre Dame. Backscatter electron images were collected using a 1 μ m beam, an accelerating voltage of 20 kV, and a probe current of 25–50 nA. Microprobe analyses were performed using a 10 μ m defocused beam, accelerating voltage of 15 kV, a probe current of 20 nA, 15 s on-peak counting time, and two background measurements per peak. Sodium was measured first to minimize loss via volatilization. During core to rim line scans, a point was measured every 6 μ m using a 5 μ m diameter beam. Microprobe data were corrected for matrix effects using a ZAF correction routine. Analysis points near Ferich inclusions were avoided. The quality of EPMA data was monitored by major element oxide and cation totals. Data points where major element oxide totals were greater than 101.5% or less than 98.5% are not used in further discussion nor are points with cation totals greater or less than 20 ± 0.1 cations (based on 32 O).

3.2. Laser Ablation Inductively Coupled Plasma Mass Spectrometry (LA-ICP-MS)

Scandium, Ti, V, Rb, Sr, Y, Ba, La, Ce, Nd, Sm, Eu, and Pb were measured in plagioclase crystals using a New Wave UP-213 UV laser ablation system interfaced with a ThermoFinnigan Element 2 ICP-MS operated in fast magnet scanning mode at the University of Notre Dame. We used a laser frequency of 5 Hz, pulse energy of 0.02–0.03 mJ pulse⁻¹, 30 μ m diameter pits, and helium as the carrier gas (~0.7 l min⁻¹) mixed with argon (~1.0 l min⁻¹) before introduction to the plasma. Due to the transient nature of the laser ablation signal, analyses were conducted in

peak jumping mode with one point quantified per mass. The LA-ICP-MS spots were coincident with previous EPMA analyses, and Ca measured by EPMA was used as an internal standard for each spot analysis. The trace element glass NIST 612 was used as a calibration standard for all laser ablation analyses. Although Egginis and Shelley (2002) noted heterogeneity of certain elements in NIST 612 glass, they considered it a reliable calibration standard for the elements examined in this study. The analytical protocols of Longerich (1996) were used for LA-ICP-MS data reduction. A more complete description of the EPMA and LA-ICP-MS methods are provided by Kinman and Neal (2006). To assess data quality all laser ablation analyses were collected in time-resolved mode so that signal from inclusions and alteration-filled fractures could be easily identified. Results from laser ablation spots close to fractures or that penetrated into underlying fractures were discarded. The rate of laser ablation was tested using a 100 μm thick plagioclase wafer prior to sampling, which allowed optimization of operating conditions to yield desired sensitivity and sampling depth (<30 μm).

3.3. Microdrilling and Sr isotope microanalysis

Microdrilling for Sr isotope microanalysis was performed using a Merchantek MicroMill in the Arthur Holmes Isotope Geology Laboratory at the University of Durham (UK) after completion of EPMA and LA-ICP-MS work. The micro-sampling, micro dissolution and Sr separation techniques detailed in Charlier et al. (2006) were followed. The samples were run on Re filaments with a TaF activator, and $^{87}\text{Sr}/^{86}\text{Sr}$ ratios were measured using a Finnigan Triton thermal ionization mass spectrometer (TIMS). Charlier et al. (2006) and Font et al. (2007) provide detailed descriptions of the micro-Sr isotope method.

3.4. Choosing partition coefficients (D)

Choosing an appropriate trace element partition coefficient is critical to the accuracy of the inverted magma composition and the petrologic interpretations made with it. Blundy (1997) noted that inversion of magma compositions from mineral data using appropriate trace element D values is a robust means of estimating parent magma compositions and suggested that trace element D values derived from microbeam techniques were more accurate than those derived from bulk crystal-matrix analyses. Blundy and Wood (1991, 1994) and Bindeman et al. (1998) showed that the dominant factors controlling the trace element D values for plagioclase are An content and crystallization temperature. Bindeman et al. (1998) applied this relationship to a variety of major and trace elements and produced values for the constants “ a ” and “ b ” in their Eq. (2) (Eq. (1) below) for calculating plagioclase partition coefficients via the expression:

$$RT \ln(D_i) = aX_{\text{An}} + b \quad (1)$$

where R is the gas constant, T is temperature (Kelvin), i is the element of interest, and X_{An} is the mole fraction of anorthite. Using Eq. (1), Ginibre et al. (2002) noted that temperatures in the range of 850–1000 $^{\circ}\text{C}$ had miniscule effect on calculated melt concentrations for Sr and Ba (within their analytical uncertainty). Likewise, Bindeman et al. (1998) showed that variations of ~ 150 $^{\circ}\text{C}$ produce <10% differences for particular partition coefficients, which were often within error of each other.

Blundy and Wood (1994) presented an alternative model for quantitative prediction of D values based upon thermodynamic principles and lattice strain theory (Brice, 1975). Specifically, they noted the dominant roles of cation size, lattice site size, and elasticity of the lattice site related to cation substitution in minerals. The elastic response of a lattice site to cation substitution is measured by Young's Modulus (E), and the value of E_{plag} is dependent upon plagioclase An content and the charge of the substituent cation (Blundy and Wood,

1994, 2003). Eq. (2) (Blundy and Wood, 1994, Eq. (3)) is the basis of their predictive D model that we apply to plagioclase,

$$D_i = D_0^{z+} \exp \left[\frac{-4\pi E_{\text{plag}} N_A \left[\frac{r_o}{2} (r_o^2 - r_i^2) + \frac{1}{3} (r_i^3 - r_o^3) \right]}{RT} \right] \quad (2)$$

where D_i of a trace element (i) is a function of the strain compensated partition coefficient for the divalent (D_0^{2+}) or trivalent (D_0^{3+}) substituent cation, Young's Modulus for the plagioclase M lattice site (E_{plag}), N_A (Avogadro's Number), the radius of the plagioclase M site (r_o), the radius of the substituent cation (r_i), the gas constant (R), and crystallization temperature (T). For a more thorough discussion of this model see Blundy and Wood (1994, 2003).

3.5. Partition coefficients for Elan Bank plagioclase crystals

Eq. (2) and the parameterizations of Blundy and Wood (1994, 2003) were used to calculate D values for Rb, Sr, Y, Ba, La, Ce, Pr, Nd, and Sm, as partitioning of these elements are the better constrained through experimental studies. Estimates of D_{Sc} are unrealistically low (<0.001) using the Blundy and Wood (1994) method, which is most likely due to inadequate estimation of the strain-free partition coefficient. The partitioning behavior of Fe and Eu are strongly affected by oxygen fugacity fO_2 , and due to a lack of fO_2 constraints, no attempt was made to estimate D_{Fe} or D_{Eu} values. Magnesium is known to substitute in more than one plagioclase cation site, and based upon this complex partitioning D_{Mg} was not calculated (Bindeman et al., 1998). Blundy and Wood (1994) noted that predictive approaches are inaccurate for Pb, which has a lone pair of free electrons. A

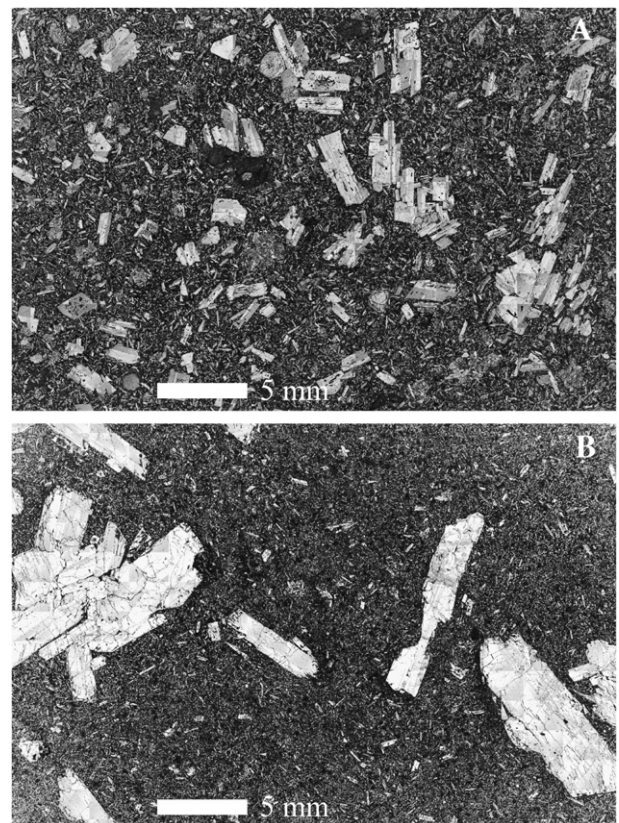


Fig. 3. Cross polarized light petrographic thin section photographs of the A) the Unit 4 basalt (183-1137A-32R-05W-22-27), and B) the Unit 10 basalt (183-1137A-46R-01W-20-35). Plagioclase phenocrysts in the Unit 4 basalt occur as individual euhedral crystals and as glomerocrysts. Plagioclase phenocrysts in the Unit 10 basalt occur most commonly as parts of glomerocrysts.

crystallization temperature of 1150 °C was assumed to calculate *D* values. The validity of this assumption was examined using the MELTS program (Ghiorso and Sack, 1995; Asimow and Ghiorso, 1998) to determine the temperature at which plagioclase arrives on the liquidus during crystallization of a typical Elan Bank basalt whole-rock composition. We input four upper group and lower group Site 1137 whole-rock basalt compositions with 4.4 wt.% MgO, 5.9 wt.% MgO, 6.0 wt.% MgO, and 7.3 wt.% MgO reported by Shipboard Scientific Party (2000) into the MELTS program. During equilibrium crystallization, plagioclase appeared on the liquidus at 1080 °C for the lowest MgO basalt and at 1180 °C from the highest MgO basalt. The use of 1080 °C versus 1180 °C in *D* calculations yields <10% differences in trace element concentrations of parent liquids, which is within the

analytical error for the LA-ICP-MS and EPMA analyses of the elements of interest.

The effects of pressure on plagioclase *D* values are not well documented for most elements. VanderAuwera et al. (2000) referred to the effect of pressure on D_{Sr} as “relatively minor”. A crystallization pressure of 0.001 kbar was assumed for *D* calculations. It was assumed that the strain compensated (i.e., strain free) partition coefficient D_0^{2+} in plagioclase is best approximated by D_{Ca} (Blundy and Wood, 2003). Eq. (1) and the “*a*” and “*b*” constants reported for Ca by Bindeman et al. (1998) were used to estimate D_{Ca} . Eq. (1) and the “*a*” and “*b*” constants reported for Na by Bindeman et al. (1998) were used to estimate D_0^{3+} . Estimation of D_0^{3+} is less straightforward. D_0^{3+} was assumed to be ~7.5% of D_0^{2+} , which was derived from experimental

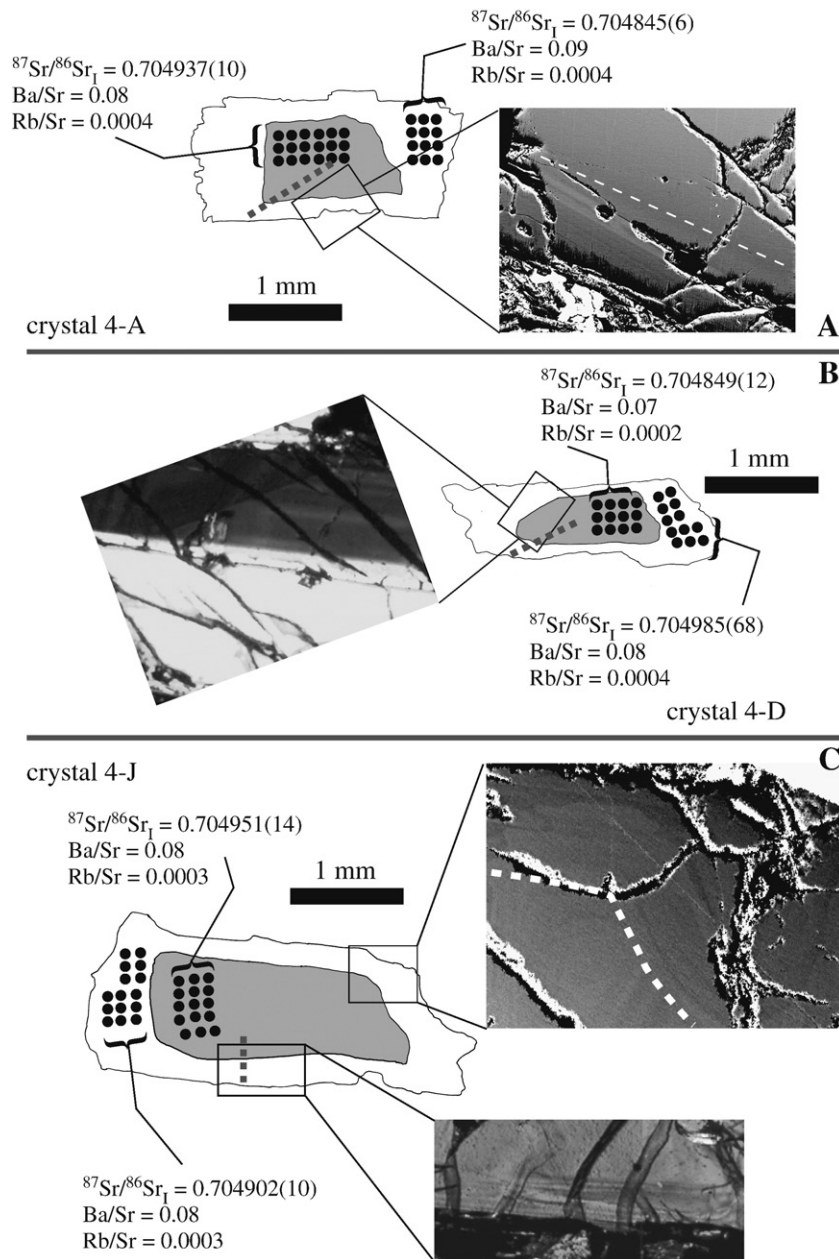


Fig. 4. Diagrams of zoning features in three of the five Unit 4 plagioclase phenocrysts that were subjects of EPMA, LA-ICP-MS and micro-Sr isotope analyses. Thin dotted black lines mark the locations of core to rim EPMA transects. Black dots are approximate microdrill sampling locations. $^{87}Sr/^{86}Sr_I$ results are shown for each along with the measured 2σ error in parentheses. Measured Ba/Sr and Rb/Sr ratios are shown for each zone examined. A) The core of crystal A is bounded by a resorption surface that is marked with a dotted white line. Anorthite content increases from ~An₆₅ to >An₇₀ (see Fig. 7A). B) The core of crystal D is bounded by a resorption surface with a change from ~An₆₃ to >An₆₇ across the surface (see Fig. 7C). C) Crystal J is a normal zoned crystal. There is a change in the zoning pattern noted by a white dotted line but no obvious resorption surface (see also Fig. 7J).

data reported in Blundy (1997). Eq. (1) and the “a” and “b” constants reported for Ti by Bindeman et al. (1998) were used to estimate D_{Ti} .

4. Results

4.1. Petrography

Plagioclase phenocrysts are more ubiquitous in the Unit 4 basalt than in the Unit 10 basalt Fig. 3. Unit 4 plagioclase phenocrysts are typically euhedral, commonly occur as individual crystals and less frequently as clusters of crystals. Unit 10 plagioclase phenocrysts are

large relative to Unit 4 phenocrysts and occur primarily as clusters of euhedral to sub-rounded crystals. Plagioclase phenocrysts from both Units 4 and 10 exhibit distinct zonation in cross polarized light (e.g., Figs. 3, 4, 5). The interiors of plagioclase phenocrysts frequently exhibit oscillatory type zoning (e.g., crystal 10-1D-A; Fig. 5), and most have obvious core and rim sections. Sections of zoned plagioclase crystals are divided into three types: 1) cores, 2) intermediate zones, and 3) rims. Dissolution surfaces are abundant in crystals from both Units 4 and 10, and frequently enclose crystal core regions (e.g., Fig. 5). Glass and partially crystallized inclusions are present along some dissolution surfaces. It is important to note that the labeling of cores

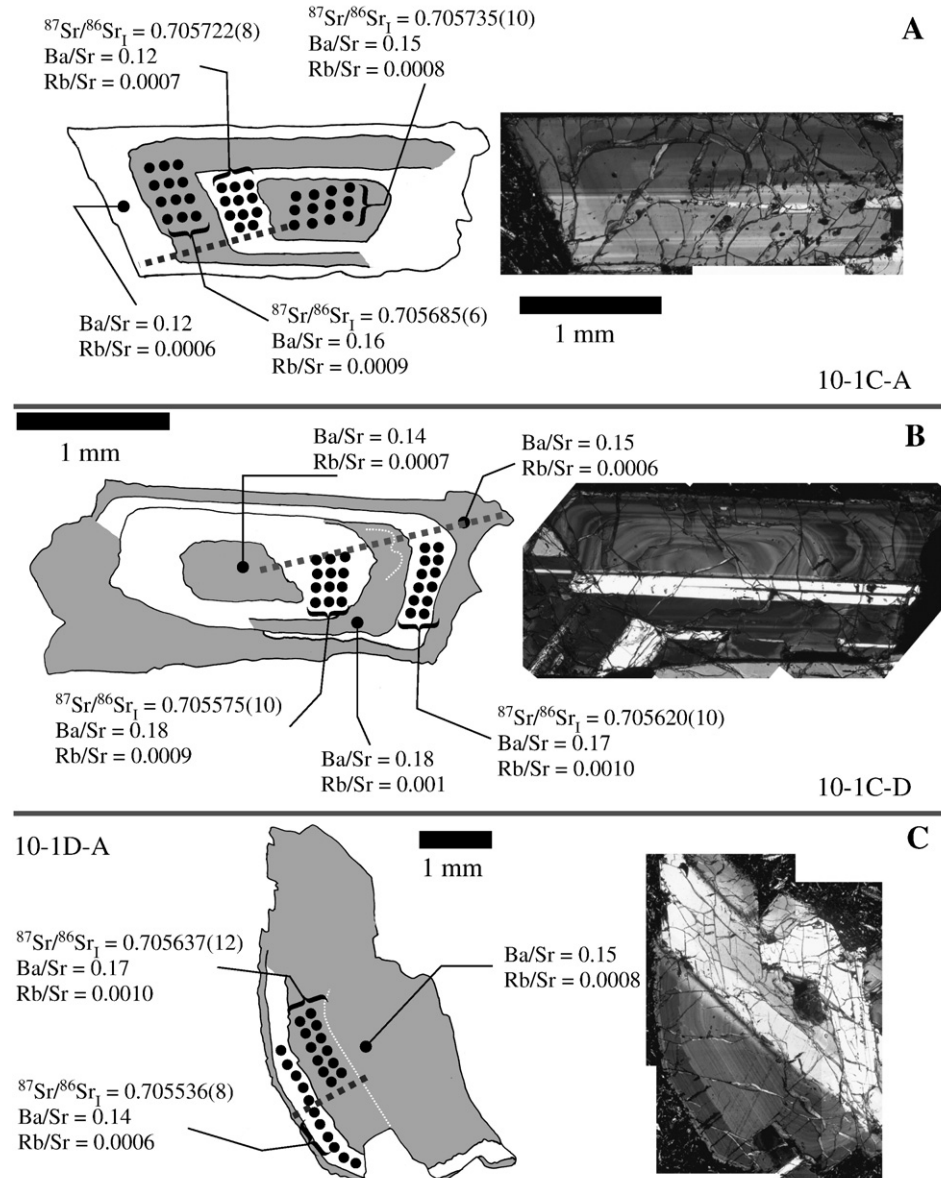


Fig. 5. Diagrams of zoning features in five Unit 10 plagioclase phenocrysts that were subjects of EPMA, LA-ICP-MS and micro-Sr isotope analyses. Thin dotted black lines mark the locations of core to rim EPMA transects. Black dots are approximate microdrill sampling locations. $^{87}\text{Sr}/^{86}\text{Sr}_i$ results are shown for each along with the measured 2σ error in parentheses. Measured Ba/Sr and Rb/Sr ratios are shown for each zone examined. A) Crystal 10-1C-A contains four distinct zones that were sampled. These zones, which were each sampled, are $\sim\text{An}_{60}$ in the core, an $\sim\text{An}_{65}$ intermediate zone, an $\sim\text{An}_{60}$ intermediate zone, and an $>\text{An}_{65}$ rim zone (see Fig. 8B). B) Crystal 10-1C-D contains abundant oscillatory zoning but has an overall reverse zonation pattern and at least two zones, which were each sampled, where An content is higher (up to An_{65}) than the core An_{61-62} (see Fig. 8F). C) Crystal 10-1D-A appears to be a fragment of a large crystal with an oscillatory zoned interior. This crystal has an obvious resorption surface near the rim that is accompanied by a change in from An_{62-63} to $>\text{An}_{66}$. Diagrams of zoning features in the two Unit 10 plagioclase phenocrysts that were subjects of EPMA, LA-ICP-MS and micro-Sr isotope analyses. Thin dotted black lines mark the locations of core to rim EPMA transects. $^{87}\text{Sr}/^{86}\text{Sr}_i$ results are shown for each along with the measured 2σ error in parentheses. Measured Ba/Sr and Rb/Sr ratios are shown for each zone examined. D) Crystal 10-2A-C has an $\sim\text{An}_{60}$ core bounded by a resorption surface and an An_{65-66} rim. Both the core and rim were sampled. E) Crystal 10-2A-D has an $\sim\text{An}_{60}$ core bounded by a dissolution surface and an An_{65-67} rim. Both the core and rim were sampled.

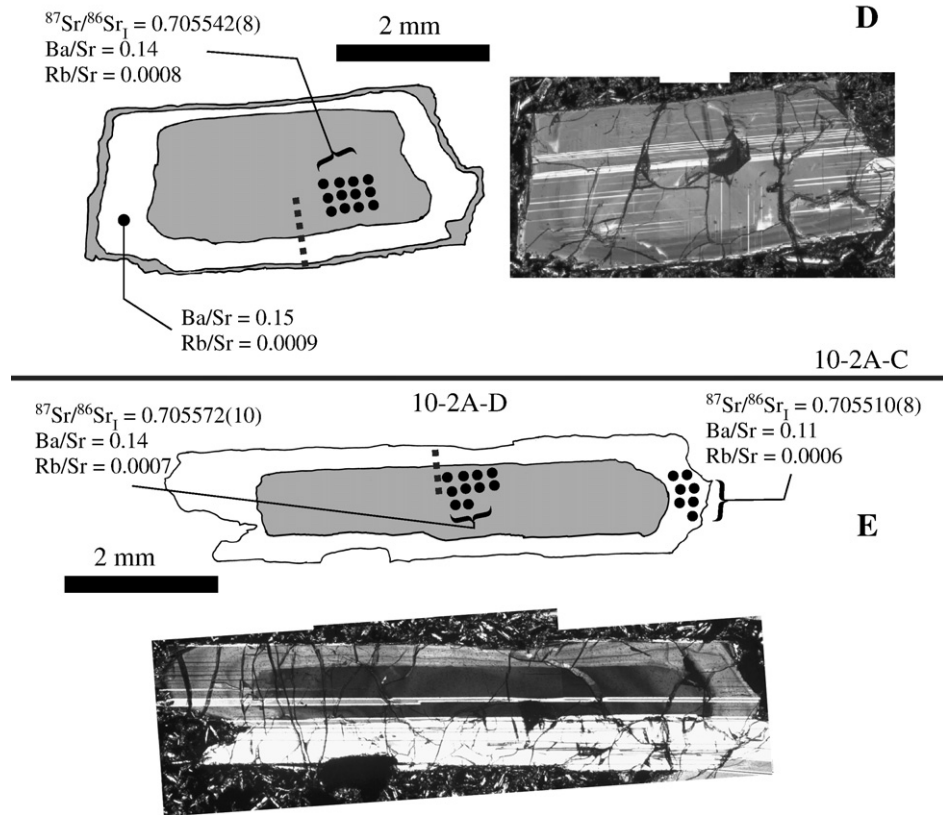


Fig. 5 (continued).

and intermediate zones only applies to the two dimensional crystal as seen in thin section. They may not represent the true zones in the crystal due to geometric distortions introduced during sectioning of

basalt samples, which makes it difficult to know when a true crystal core is being sampled (Wallace and Bergantz, 2004).

4.2. Major elements

The An–Ab–Or compositions of zones within Unit 4 and 10 plagioclase phenocrysts that were targeted for compositional microanalysis are shown in Figs. 6, 7, 8. The An content of Unit 4 plagioclase zones range from An₅₄ to An₇₁. Unit 10 crystals overlap those from Unit 4 but span a narrower range (An₅₇ to An₆₇). Unit 4 plagioclase cores trend to higher An contents, and rims trend to lower An contents and greater Or content (Fig. 6A). Intermediate zones are nearly identical to Unit 4 cores in terms of An–Ab–Or composition (Fig. 6B). The lowest An zone sampled in a Unit 4 plagioclase was An₅₄ along a crystal rim, whereas the highest An zones are an An₇₁ intermediate zone near a crystal core and an An₇₁ core. Unit 10 plagioclase cores and intermediate zones trend to lower An content than rim zones (Fig. 6B). The highest An zones sampled in Unit 10 plagioclase phenocrysts are an An₆₇ rim zone and an An₆₇ intermediate zone that is adjacent to a crystal rim, and the lowest An zones sampled include two interior An₅₇ zones and an An₅₈ crystal core (Fig. 6B).

Core to rim EPMA point traverses reveal that each of the Unit 4 and 10 plagioclase crystals analyzed in this study contain major element oscillations, which is consistent with oscillatory zoning apparent in cross polarized light and backscatter electron images (e.g., Fig. 5B,C). Half of the Unit 4 plagioclase phenocrysts examined exhibit normal zoning patterns (Fig. 7B,D,G,H,J). Crystals from Units 4 and 10 have ubiquitous thin (5–10 μm) low An rims that are not obvious for each crystal in Figs. 7 and 8. One Unit 4 crystal examined in this study exhibits little core to rim change in An content but has an overall An content similar to interior sections of other Unit 4 crystals (Fig. 7C). This crystal may be an example of a geometric

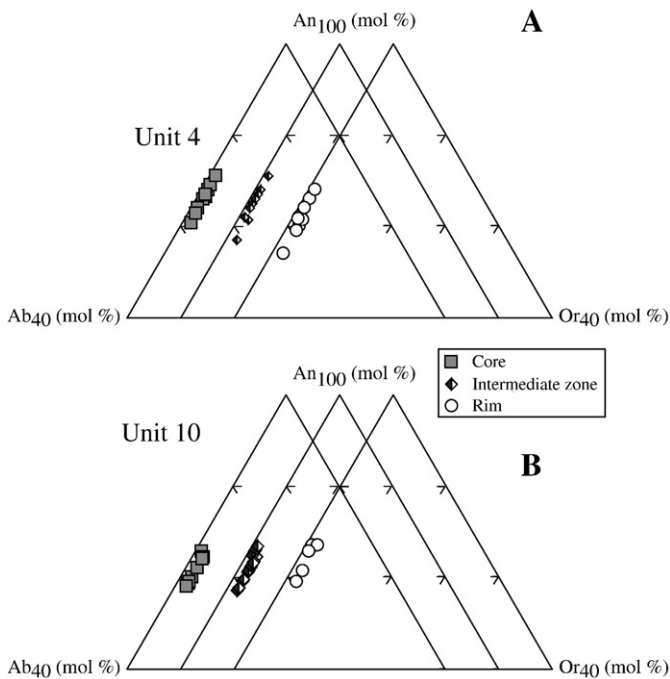


Fig. 6. A) An–Ab–Or compositions of Unit 4 plagioclase phenocryst core, intermediate, and rim zones. Unit 4 rim zones trend to the lowest An contents. B) An–Ab–Or compositions of Unit 10 plagioclase phenocryst core, intermediate, and rim zones. Unit 10 plagioclase cores trend to the lowest An contents of all zones sampled.

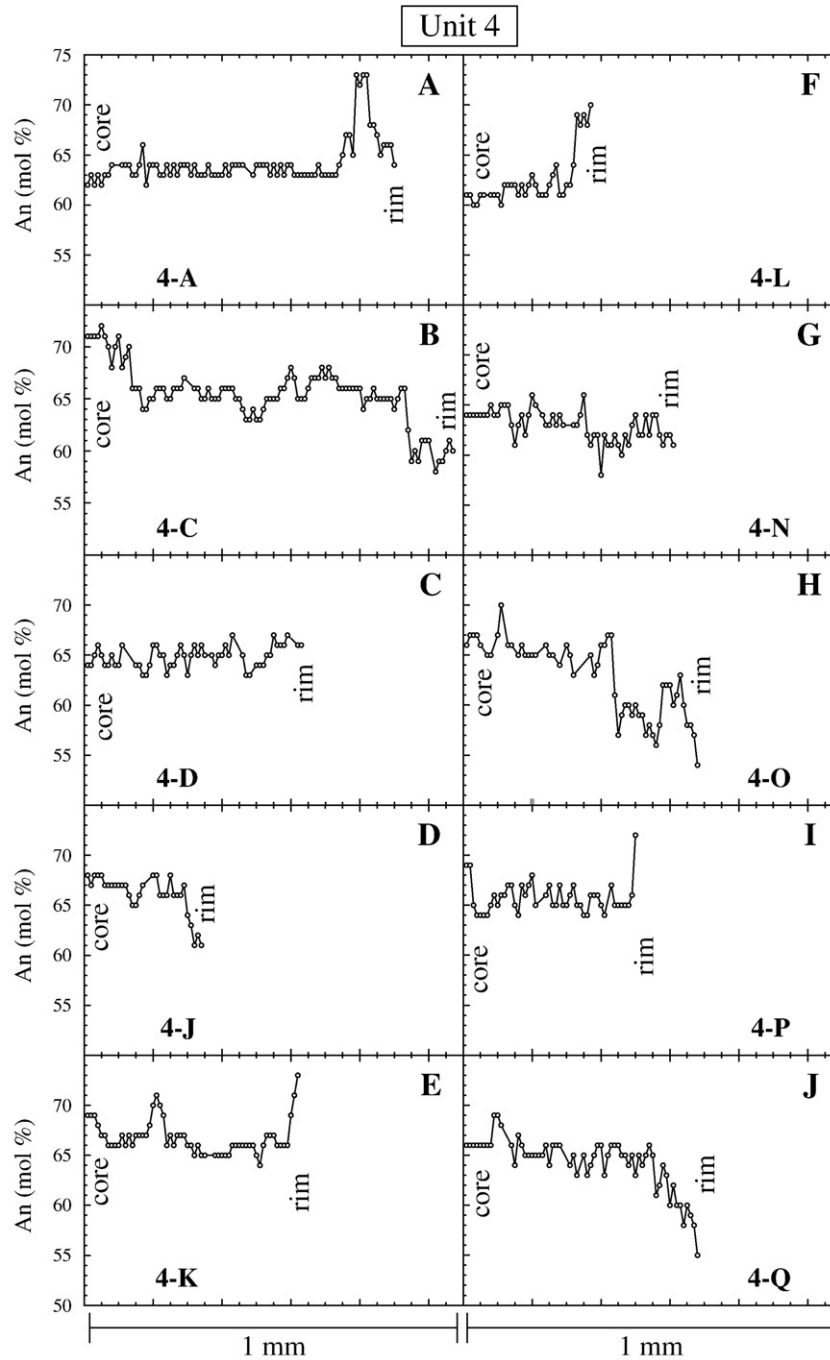


Fig. 7. Core to rim profiles of ten Unit 4 plagioclase phenocrysts. Other major and trace element data measured at various points along the core to rim transects are presented in Table 1.

distortion introduced during sectioning of the crystal. Four of the ten Unit 4 plagioclase phenocrysts examined in this study exhibit reverse zonation (Fig. 7A,E,F,I). With one exception (10-1C-B2; Fig. 8D), each of the Unit 10 crystals exhibits reverse zonation (Fig. 8). In summary, Unit 4 plagioclase phenocrysts are a mixture of normal zoned crystals, reverse zoned crystals, and a few unzoned crystals. Unit 10 plagioclase phenocrysts dominantly exhibit reverse zonation.

4.3. Trace elements

Comparisons of measured trace element abundances in core, rim, and intermediate zones with similar An contents are most informative, as observed differences here are less likely related to plagioclase

composition alone (Blundy and Wood, 1991). Given the narrow An range exhibited by Unit 4 and 10 crystals, this manner of comparison is useful.

4.3.1. Scandium, Ti, V, and Pb

Negative correlations of Ti, V, and Pb abundance with An content are apparent for crystals from both Units 4 and 10. There is little obvious correlation of Sc abundance with An content for crystals from either Unit (Fig. 9A–C,E; Tables 4, 5). In terms of Sc abundance there is little distinction between Unit 4 and Unit 10 plagioclase crystals (Fig. 9A). For a given An content, Unit 10 phenocrysts have greater Ti, V, and Pb abundances than Unit 4 plagioclase crystals (Fig. 9B,C,F). There is little distinction in Sc, Ti, V, and Pb abundances among plagioclase zones within either Unit.

Table 1

Unit 4 plagioclase major and trace element abundances 1 = zone; 2 = FeOT; 3 = An (Mol%).

Sample	Zone	An (mol%)	FeO _T	P ₂ O ₅	K ₂ O	TiO ₂	Na ₂ O	CaO	MgO	SiO ₂	Al ₂ O ₃	Total	Sc	Ti	V	Rb	Sr	Y	Ba	La	Ce	Pr	Nd	Sm	Eu	Pb
4-K	C	69	0.62	0.12	0.18	0.05	3.47	14.29	0.16	51.0	31.0	100.95	2.0	642	3.5	0.37	829	0.33	99	0.92	2.2	0.21	0.77	0.07	0.59	0.76
4-K	I	71	0.67	0.08	0.17	0.04	3.17	14.78	0.18	50.6	31.2	100.91	1.4	522	3.3	0.22	850	0.27	81	1.07	2.4	0.23	1.03	0.15	0.61	0.67
4-K	R	66	0.67	0.05	0.21	0.09	3.78	13.7	0.18	51.5	30.8	100.99	1.9	565	3.1	0.17	839	0.17	79	0.95	2.0	0.20	0.68	0.09	0.59	0.60
4-L	C	61	0.63	0.10	0.25	0.09	4.23	12.41	0.19	52.9	29.9	100.73	1.2	566	2.8	0.30	797	0.07	73	0.94	1.7	0.18	0.52	0.14	0.52	0.55
4-L	I	62	0.68	0.10	0.27	0.10	4.23	12.8	0.20	52.7	29.7	100.84	1.4	630	3.4	0.42	804	0.33	84	0.77	1.7	0.16	0.48	0.14	0.63	0.67
4-L	R	68	0.65	0.09	0.18	0.08	3.55	14.17	0.17	50.9	31.0	100.79	1.1	481	3.8	0.23	803	0.23	68	0.84	1.8	0.18	0.67	0.16	0.53	0.71
4-Q	C	66	0.60	0.07	0.24	0.07	3.70	13.68	0.18	52.0	30.1	100.59	1.5	478	5.1	0.34	852	0.12	70	0.74	1.8	0.16	0.48	0.10	0.63	0.86
4-Q	I	65	0.65	0.08	0.22	0.03	3.90	13.37	0.18	52.5	29.5	100.49	1.6	483	4.0	0.24	882	0.13	69	0.87	1.8	0.17	0.70	0.05	0.55	0.70
4-Q	R	60	0.73	0.05	0.26	0.08	4.34	12.47	0.16	53.4	28.9	100.39	2.8	581	3.4	–	922	0.08	91	1.01	2.0	0.23	0.73	0.12	0.59	0.78
4-P	C	66	0.65	0.10	0.21	–	3.63	13.34	0.18	52.1	30.2	100.48	2.1	445	3.8	0.34	856	0.14	68	0.69	1.5	0.16	0.48	0.07	0.51	0.89
4-P	I	65	0.60	0.08	0.21	–	3.82	13.04	0.15	53.0	29.9	100.17	1.4	462	4.6	0.35	825	0.13	67	0.78	1.8	0.17	0.69	0.07	0.56	0.65
4-J	C	68	0.60	0.04	0.20	0.08	3.60	14.43	0.20	51.3	30.4	100.92	1.5	499	4.4	0.30	924	0.09	71	0.86	1.8	0.20	0.61	0.08	0.58	0.44
4-J	I	68	0.62	0.09	0.19	0.08	3.66	14.26	0.17	51.4	30.7	101.21	1.6	479	4.2	0.29	909	0.10	72	0.90	1.9	0.17	0.57	0.12	0.55	0.48
4-J	R	62	0.79	0.08	0.25	0.07	4.23	12.91	0.19	53.0	29.4	100.90	1.8	580	3.9	0.34	925	0.09	98	1.05	1.9	0.20	0.68	0.05	0.73	0.64
4-N	C	64	0.65	0.08	0.20	0.28	3.92	13.22	0.19	52.4	30.0	100.94	1.7	501	3.3	0.26	849	0.10	70	0.84	1.7	0.18	0.66	0.14	0.57	0.63
4-N	R	61	0.80	0.06	0.26	–	4.23	12.71	0.19	52.9	29.7	100.88	1.5	845	6.9	0.59	1040	0.21	132	1.53	2.8	0.26	1.22	0.21	1.33	0.97
4-O	C	67	1.24	0.07	0.20	–	3.57	13.57	0.18	51.1	31.0	100.97	1.2	429	3.8	0.31	874	0.13	69	0.84	1.8	0.14	0.68	0.10	0.61	0.54
4-O	I	67	0.68	0.11	0.20	0.04	3.58	13.43	0.16	51.9	30.7	100.72	2.2	535	4.1	0.40	934	0.11	92	0.96	1.9	0.19	0.73	0.10	0.72	0.82
4-O	I	57	0.71	0.06	0.30	0.09	4.60	11.60	0.16	54.2	29.1	100.73	1.5	660	3.5	0.51	905	0.10	91	0.92	2.1	0.21	0.80	0.10	0.55	0.53
4-O	I	62	0.73	0.10	0.25	0.11	4.09	12.56	0.16	53.0	29.6	100.62	1.2	713	4.9	0.48	983	0.10	116	1.26	2.3	0.20	0.93	0.20	0.90	0.67
4-O	R	54	0.87	0.09	0.33	0.13	4.83	10.67	0.38	55.2	28.0	100.46	2.0	785	7.2	0.69	917	0.13	125	1.15	2.1	0.20	0.72	0.15	0.98	0.69
4-D	C	67	0.67	0.10	0.20	–	3.65	13.98	0.17	51.6	30.3	100.70	1.1	522	4.0	0.18	929	0.13	69	0.88	1.7	0.18	0.77	0.12	0.59	0.46
4-D	R	64	0.60	0.08	0.21	0.07	3.96	12.90	0.19	52.1	30.0	100.13	1.5	534	4.5	0.34	906	0.12	71	0.88	1.6	0.17	0.56	0.10	0.64	0.48
4-A	C	63	0.60	0.08	0.22	0.09	4.10	12.83	0.19	53.0	29.2	100.21	1.7	492	3.0	0.36	949	0.08	77	0.87	1.8	0.19	0.64	0.10	0.44	1.21
4-A	I	64	0.65	0.06	0.22	0.08	4.07	13.28	0.19	52.7	29.0	100.24	2.0	519	3.6	0.40	929	0.09	84	0.82	2.1	0.20	0.64	0.07	0.57	0.53
4-A	I	64	0.68	0.07	0.22	0.08	4.01	13.30	0.21	52.9	28.8	100.23	2.4	525	3.4	0.36	942	0.11	80	0.88	2.1	0.22	0.73	0.10	0.60	0.46
4-A	R	64	0.71	0.08	0.23	0.09	3.85	12.84	0.17	52.8	28.9	99.66	2.2	474	3.9	0.33	836	0.10	73	0.74	1.8	0.16	0.60	0.12	0.60	0.46
4-C	C	71	0.65	0.08	0.18	0.04	3.24	15.04	0.14	50.5	30.3	100.16	1.2	447	3.2	0.27	945	0.21	89	1.05	2.2	0.22	0.87	0.09	0.59	0.67
4-C	I	66	0.60	0.07	0.20	0.09	3.80	13.78	0.18	52.3	29.2	100.15	1.5	502	3.5	0.31	904	0.15	74	0.99	1.9	0.18	0.78	0.11	0.55	0.64
4-C	R	59	0.69	0.05	0.28	0.07	4.58	12.52	0.17	53.7	28.3	100.31	2.4	594	3.8	0.60	904	0.09	97	1.00	2.0	0.21	0.61	0.08	0.65	0.68

¹C = core; I = intermediate zone; R = rim.²Total Fe as FeO.³[An = Ca / (Ca + Na + K)] * 100.

4.3.2. Barium, Sr, and Rb

Crystals from Units 4 and 10 exhibit negative correlations of Ba and Rb with An content and no correlation of Sr abundance with An content as Tepley et al. (2000) found at El Chichón volcano, Mexico (Fig. 9A,D,E). At a given An content, Unit 10 crystals have greater Ba and Rb abundances than Unit 4 phenocrysts. Unit 10 crystals tend to have lower Sr than Unit 4 crystals at a given An content (Fig. 9G). Where Unit 10 crystal interiors (cores and intermediate zones) and rims have similar An content, rims tend to have the lowest Ba and Rb (Fig. 9D,E).

4.3.3. Yttrium and the rare earth elements La, Ce, Pr, Nd, Sm, and Eu

The highest Y abundances were measured in Unit 4 crystal cores and intermediate zones (Fig. 9H). There is no other obvious systematic variation in Y abundance between phenocryst zones in crystals from either Unit. At a given An content, Unit 10 phenocrysts have greater La, Ce, Pr, Nd, Sm, and Eu. Where interior and rim zones of Unit 4 crystals have similar An content, the interior zones have lower overall REE abundances (Fig. 9). The opposite relationship holds true for Unit 10 phenocryst zones with overlapping An, where interior zones tend to have greater REE abundances (Fig. 9).

4.4. Sr isotope microdrilling

Measured ⁸⁷Sr/⁸⁶Sr ratios were age corrected to obtain ⁸⁷Sr/⁸⁶Sr_t assuming an age of 107.7 Ma and Rb/Sr ratios measured via LA-ICP-MS at coincident drill sites (Duncan, 2002). The crystals examined generally have Rb/Sr < 0.001. There are subtle variations in ⁸⁷Sr/⁸⁶Sr_t between crystal zones in Unit 4 and 10 crystals (Figs. 4, 5, 10; Table 3). Unit 4 crystals have less radiogenic ⁸⁷Sr/⁸⁶Sr_t than Unit 10 crystals (Fig. 10). The rim of Unit 4 crystal D bears the most radiogenic ⁸⁷Sr/⁸⁶Sr_t observed in a Unit 4 crystal and exhibits a higher ⁸⁷Sr/⁸⁶Sr_t than all Site 1137 upper group whole-rock samples reported by Ingle

et al. (2002b) (Fig. 4B). All other Unit 4 plagioclase zones overlap Site 1137 upper group whole-rock ⁸⁷Sr/⁸⁶Sr_t reported by Ingle et al. (2002b). There is little other distinction in terms of ⁸⁷Sr/⁸⁶Sr_t between core, intermediate, and rim zones (Fig. 10).

Site 1137 lower group whole-rock samples reported by Ingle et al. (2002b) extend to more radiogenic ⁸⁷Sr/⁸⁶Sr_t than any Unit 10 plagioclase zone sampled in this study (Fig. 10). Unit 10 plagioclase rims exhibit the least radiogenic ⁸⁷Sr/⁸⁶Sr_t of the three zones (Fig. 10). The core of crystal 10-1C-A has the most radiogenic ⁸⁷Sr/⁸⁶Sr_t of any Unit 10 crystal zone sampled (Fig. 5A), and the rim of crystal 10-2A-D has the least ⁸⁷Sr/⁸⁶Sr_t of any Unit 10 crystal zone (Fig. 5B). In summary, crystals from both Units 4 and 10 have ⁸⁷Sr/⁸⁶Sr_t similar to Site 1137 upper group (less radiogenic) and lower group (more radiogenic) whole-rock samples (i.e., their host basalts) reported by Ingle et al. (2002b).

4.5. Inferred parent magma compositions

Calculated plagioclase parent magmas from Units 4 and 10 have Ba/Sr ratios and Rb abundances that overlap Site 1137 upper group and lower group basalts (Fig. 11), although this overlap is less apparent when a smaller subset of Site 1137 basalts are considered (i.e., those where ⁸⁷Sr/⁸⁶Sr ratios were also measured) (Fig. 11B). Rare earth element abundances (including Y) in Unit 4 and 10 plagioclase parent magmas are lower than Site 1137 basalts (Tables 4, 5; Fig. 11C). The origins of these low abundances are explored below.

5. Discussion

5.1. Compositional differences between unit 4 and 10 basalts – crustal assimilation or unique mantle sources?

It is clear from previous studies that the compositions of Unit 4 and 10 basalts are distinct from one another, and the consensus view

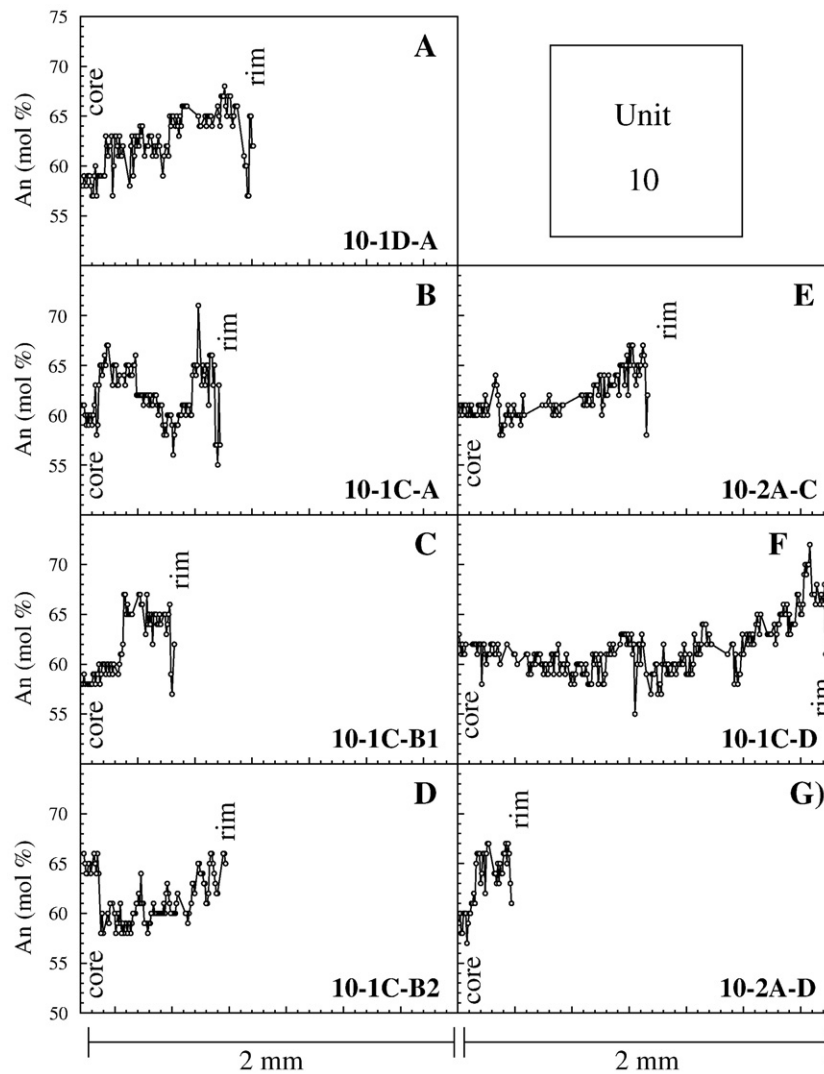


Fig. 8. Core to rim profiles of seven Unit 10 plagioclase phenocrysts. Other major and trace element data measured at various points along the core to rim transects are presented in Table 2.

is that the difference is due to a greater contribution of continental crust in lower group magmas relative to upper group magmas (Frey et al., 2000; Ingle et al., 2002b; Neal et al., 2002). Unit 10 basalts exhibit extreme Sr–Nd–Pb isotope characteristics and relative Nb and Ta depletions, which are indicative of a crustal component (Frey et al., 2000; Weis et al., 2001). The origin of crustal rocks within the Indian oceanic lithosphere and/or asthenosphere has been debated (see Frey et al. (2002) and references therein). Frey et al. (2000) suggested that a portion of Indian continental crust may have been transferred to the Antarctic plate following a ridge jump and is responsible for the presence of continental lithosphere beneath Elan Bank. Seismic and geochemical studies provide strong evidence in support of such hypotheses where they have indicated that fragments of continental lithosphere of varying age are stranded heterogeneously within the Indian Ocean lithosphere and asthenosphere (Mahoney et al., 1995; Operto and Charvis, 1996; Frey et al., 2000; Weis et al., 2001; Frey et al., 2002; Neal et al., 2002). Garnet biotite gneiss clasts recovered during drilling at Site 1137 on Elan Bank provided firm evidence for the presence of continental lithosphere beneath Elan Bank (Nicolaysen et al., 2001; Ingle et al., 2002a). Age dates of ~0.5–2.5 Ga were reported by Nicolaysen et al. (2001) for the clasts, and Ingle et al. (2002a) argued that the gneiss clasts exhibit affinities to Indian crustal rocks. These interpretations support the hypothesis of Frey et al. (2000).

The discovery of garnet–biotite gneiss clasts at Site 1137 confirmed that crustal rocks were present during the petrogenesis of the basalts examined in this study. The clasts also provide insight into the compositions of the crustal rocks that may have been assimilated by Kerguelen magmas. The $^{87}\text{Sr}/^{86}\text{Sr}_i$ of the gneiss clasts are >0.776 . If these in fact represent the crustal rocks assimilated, total assimilation must have been low, as was argued by Ingle et al. (2002b). There is overwhelming evidence that crustal assimilation is responsible for the compositional differences between the Unit 4 and 10 basalts examined in this study. There is, however, little compelling evidence to indicate that the plagioclase crystals these basalts host obtained their Sr isotope or trace element signatures via an origin other than crustally contaminated parent magmas. The origins of Unit 4 and 10 plagioclase phenocrysts as well as their petrographic and compositional features are explored to better understand the insights they provide into the petrogenetic process that were active beneath Elan Bank.

5.2. Origin of KP plagioclase major element zoning and resorption surfaces

Abrupt changes of five to greater than 10 mol% An and the presence of resorption surfaces among Unit 4 and 10 plagioclase phenocrysts indicates these crystals were variably exposed to magmas with which they were at a state of disequilibrium (e.g., Figs. 4, 5, 7, 8). Injection of

Table 2Unit 10 plagioclase major and trace element abundances 1=zone; 2=FeO_T; 3=An (Mol%); 4=TiO₂; 5=BCR-2G cert.

Sample	Zone	An (mol%)	FeO _T	P ₂ O ₅	K ₂ O	TiO ₂	Na ₂ O	CaO	MgO	SiO ₂	Al ₂ O ₃	Total	Sc	Ti	V	Rb	Sr	Y	Ba	La	Ce	Pr	Nd	Sm	Eu	Pb
10-1C-A	C	60	0.63	0.11	0.33	0.16	4.48	12.98	0.14	52.7	29.4	100.93	1.5	654	6	0.70	862	0.09	133	1.10	2.5	0.22	0.83	0.13	1.09	1.18
10-1C-A	I	65	0.58	0.09	0.27	0.03	4.03	13.85	0.14	52.0	30.1	101.09	1.9	695	4.7	0.62	890	0.13	106	1.08	2.2	0.21	0.78	0.15	0.88	1.21
10-1C-A	I	62	0.59	0.06	0.31	0.10	4.19	13.18	0.16	52.6	29.1	100.29	1.6	797	5.8	0.79	911	0.12	142	1.16	2.5	0.24	0.88	0.15	0.97	1.07
10-1C-A	R	66	0.59	0.1	0.23	0.06	3.9	14.06	0.17	51.8	29.6	100.41	1.8	648	5.3	0.54	836	0.12	96.9	1.03	2.1	0.19	0.71	0.08	0.79	1.06
10-1C-B1	C	65	0.55	0.10	0.25	0.07	3.82	13.60	0.14	52.4	28.8	99.68	1.8	779	5.9	0.67	895	0.13	142	1.16	2.8	0.27	0.99	0.13	1.22	1.16
10-1C-B1	I	61	0.56	0.11	0.27	0.08	4.31	12.96	0.15	53.7	27.8	99.86	2.5	845	6.5	0.97	905	0.17	147	1.23	2.8	0.23	0.97	0.14	1.09	1.24
10-1C-B1	I	65	0.62	0.09	0.25	0.09	3.86	13.78	0.16	51.5	29.9	100.19	2.1	695	5.8	0.50	846	0.09	112	1.07	2.6	0.22	0.82	0.15	0.97	1.15
10-1C-B1	I	64	0.64	0.11	0.23	0.05	3.92	13.29	0.17	51.9	29.5	99.78	1.9	689	5.5	0.55	804	0.14	110	1.00	2.4	0.2	0.84	0.13	0.80	1.21
10-1C-B1	R	66	0.66	0.08	0.22	0.13	3.82	14.14	0.18	51.2	29.7	100.16	2.3	731	5.4	0.47	848	0.11	111	1.07	2.6	0.22	0.87	0.09	0.88	1.15
10-1C-B2	C	58	0.59	0.06	0.37	0.12	4.61	12.35	0.16	52.8	28.4	99.46	2.2	995	7.1	1.11	913	0.20	151	1.39	3.1	0.29	0.91	0.16	0.95	1.27
10-1C-B2	I	64	0.62	0.11	0.28	0.03	4.06	13.42	0.17	52.1	29.0	99.82	1.7	701	5.3	0.57	806	0.13	105	1.04	2.5	0.23	0.90	0.12	0.80	1.24
10-1C-B2	I	62	0.63	0.09	0.29	0.07	4.33	13.2	0.15	51.8	29.1	99.63	2.2	719	5.3	0.50	800	0.13	113	1.06	2.5	0.23	0.79	0.11	0.85	1.05
10-1C-B2	R	59	0.61	0.13	0.32	0.09	4.49	12.12	0.17	52.9	28.7	99.51	2.6	761	5.1	0.88	813	0.13	113	1.02	2.2	0.21	0.68	0.08	0.71	1.30
10-2A-D	C	59	0.47	0.03	0.32	0.08	4.35	11.99	0.17	54.2	28.6	100.15	1.0	803	5	0.66	885	0.20	127	1.34	2.2	0.23	0.86	0.18	1.09	1.42
10-2A-D	R	67	0.48	0.05	0.23	0.10	3.54	13.27	0.12	52.2	29.7	99.66	1.6	636	4.1	0.47	777	0.21	85	1.21	1.9	0.2	0.75	0.12	0.75	0.78
10-2A-C	C	58	0.53	0.06	0.37	0.11	4.47	11.77	0.17	54.3	28.2	99.98	1.0	785	5.0	0.71	862	0.16	120	1.36	2.2	0.25	0.93	0.17	1.04	0.78
10-2A-C	I	62	0.48	0.11	0.32	0.06	4.07	12.61	0.19	53.4	29.1	100.29	1.3	917	5.5	0.85	941	0.20	139	1.44	2.4	0.27	0.86	0.13	1.20	0.93
10-2A-C	I	67	0.49	0.07	0.27	0.05	3.62	13.97	0.17	52.0	29.3	99.91	0.9	654	4.2	0.36	772	0.16	84	1.12	2.0	0.23	0.81	0.12	0.79	0.65
10-2A-C	R	65	0.56	0.08	0.25	0.07	3.79	13.52	0.17	52.1	29.3	99.83	1.2	755	6.2	0.46	845	0.19	101	1.30	2.1	0.23	0.81	0.15	0.99	0.89
10-1C-D	C	63	0.48	0.08	0.27	0.10	3.96	12.83	0.18	53.0	29.4	100.36	1.9	737	5.3	0.55	801	0.15	114	0.97	2.3	0.21	0.77	0.10	1.01	0.83
10-1C-D	I	60	0.47	0.08	0.32	0.12	4.38	12.20	0.20	53.6	28.0	99.35	1.7	887	6.1	0.76	801	0.07	146	1.08	2.5	0.20	0.59	0.09	0.99	0.96
10-1C-D	I	63	0.44	0.05	0.28	0.11	3.97	12.71	0.16	52.9	29.3	99.92	1.8	827	5.4	0.80	797	0.15	141	1.05	2.4	0.21	0.70	0.10	0.93	0.99
10-1C-D	I	59	0.5	0.11	0.33	0.07	4.38	11.99	0.19	53.9	27.8	99.26	2.3	911	6.5	0.86	845	0.08	143	1.05	2.5	0.23	0.94	0.11	0.95	1.00
10-1C-D	R	62	0.46	0.11	0.28	0.12	4.15	12.64	0.17	53.3	27.8	98.96	1.4	839	6.8	0.51	785	0.13	119	1.03	2.4	0.23	0.74	0.09	1.06	1.34
10-1D-A	I	57	0.53	0.09	0.34	0.14	4.48	11.42	0.17	54.8	28.8	100.68	1.5	833	5.8	0.65	797	0.11	121	1.06	2.3	0.22	0.61	0.13	0.89	0.95
10-1D-A	I	57	0.41	0.07	0.36	0.14	4.49	11.53	0.18	54.5	28.0	99.68	1.6	947	5.7	0.79	815	0.10	142	1.01	2.3	0.23	0.66	0.05	0.87	0.87
10-1D-A	R	66	0.46	0.10	0.25	0.11	3.65	13.44	0.17	52.5	29.0	99.60	1.4	803	6.1	0.52	832	0.11	118	1.02	2.5	0.26	0.69	0.13	0.82	0.70
BCR-2G	–	–	–	–	–	2.30	–	–	–	–	–	–	33.1	–	402.2	46.9	335.4	33.5	706.9	26.2	52.6	6.9	28.7	6.7	2.0	10.0
–	–	–	–	–	–	±0.36	–	–	–	–	–	–	±0.74	–	±22.9	±3.7	±16.2	±1.23	±47.2	±1.1	±3.0	±0.29	±1.7	±0.43	±0.06	±0.79
BCR-2 cert.	–	–	–	–	–	2.24	–	–	–	–	–	–	32.6	–	407	47.5	337	32.5	684	25.3	53.6	6.8	28.6	6.7	2.0	10.34

¹C = core; I = intermediate zone; R = rim.²Total Fe as FeO.³[An = Ca / (Ca + Na + K)]*100.⁴Ti was measured by EPMA.⁵BCR-2G is not yet certified. BCR-2 whole-rock powder certified values are listed.

hot recharge magma into a crystallizing magma chamber can lead to partial resorption of plagioclase and subsequent growth of higher An zones, which is a feature that was noted for select crystals from Units 4 and 10 (e.g., Fig. 7A,E,F,G; Fig. 8). In the Unit 4 basalt, reverse zoned crystals are more common in glomerocrysts, whereas normal zoned plagioclase phenocrysts appear almost exclusively as individual euhedral crystals. Individual Unit 10 plagioclase phenocrysts, which are dominantly reverse zoned, that are not present in glomerocrysts are generally sub-rounded (Fig. 3). This evidence indicates that reverse zoned crystals observed in both basalts largely originated from disaggregated glomerocrysts. This is key, as glomerocryst crystals formed earlier and potentially under different conditions. The regular occurrence of reverse zoned crystals in each basalt suggests that magmatic incorporation of plagioclase-rich debris was common beneath Elan Bank. Crystals growing within solidification fronts or crystal debris piles are insulated from the hottest portions of the magma chamber and can be out of equilibrium with magma in the chamber interior (Langmuir, 1989). Likewise, crystals captured by advancing solidification fronts or deposited along the floor during magma recharge may record

the compositions of parent magmas distinct from the magma in the chamber interior (Marsh, 1996, 2004). Crystal zoning results indicate that plagioclase phenocrysts may contain compositional information related to magma differentiation beyond bulk-rock chemistry. Strontium isotope and trace element data provide greater insight into the origins of plagioclase zoning features and the compositions of magma batches involved in KP magma differentiation.

5.3. Petrogenetic insights from plagioclase $^{87}\text{Sr}/^{86}\text{Sr}_i$ ratios

Plagioclase crystals from Units 4 and 10 exhibit narrow ranges of $^{87}\text{Sr}/^{86}\text{Sr}_i$ that overlap their respective Site 1137 upper and lower group basalts reported by Ingle et al. (2002b) (Fig. 10). This observation indicates that the disparate $^{87}\text{Sr}/^{86}\text{Sr}$ ratios of the Unit 4 and 10 basalts originated prior to crystallization of plagioclase phenocrysts. Based upon the similar Sr isotope characteristics of host basalt and plagioclase, it is logical that the more radiogenic $^{87}\text{Sr}/^{86}\text{Sr}$ recorded within the Unit 10 plagioclase crystals, relative to Unit 4 crystals, are related to greater crustal assimilation.

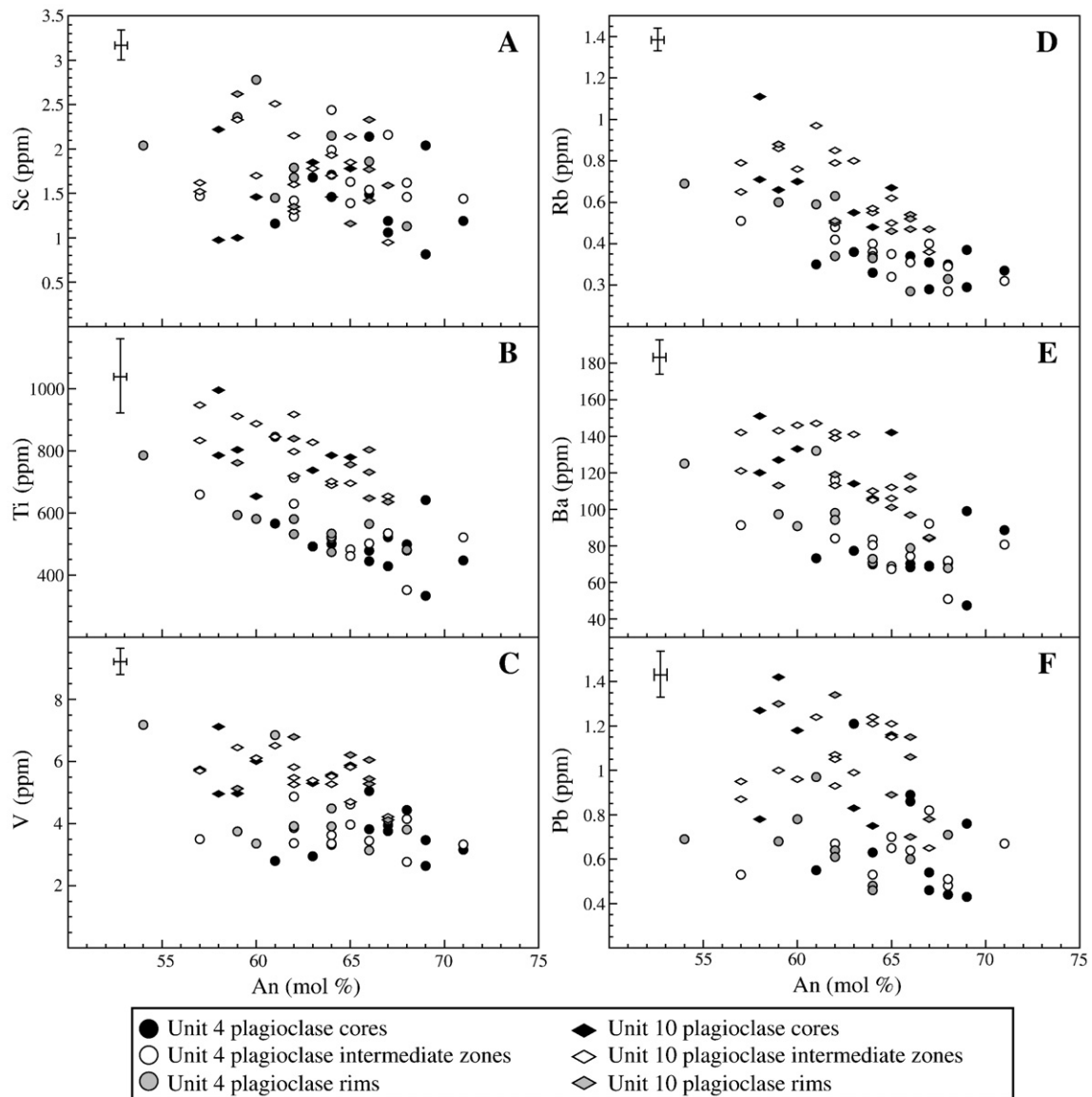


Fig. 9. Trace element abundances (in ppm) measured in core, intermediate, and rim zones of Unit 4 and 10 plagioclase phenocrysts plotted against anorthite. A) Sc, B) Ti C) V, D) Rb, E) Ba, F) Pb, G) Sr, H) Y I) La, J) Ce, K) Pr, L) Nd M) Sm, and N) Eu. Error bars represent measured 2σ error.

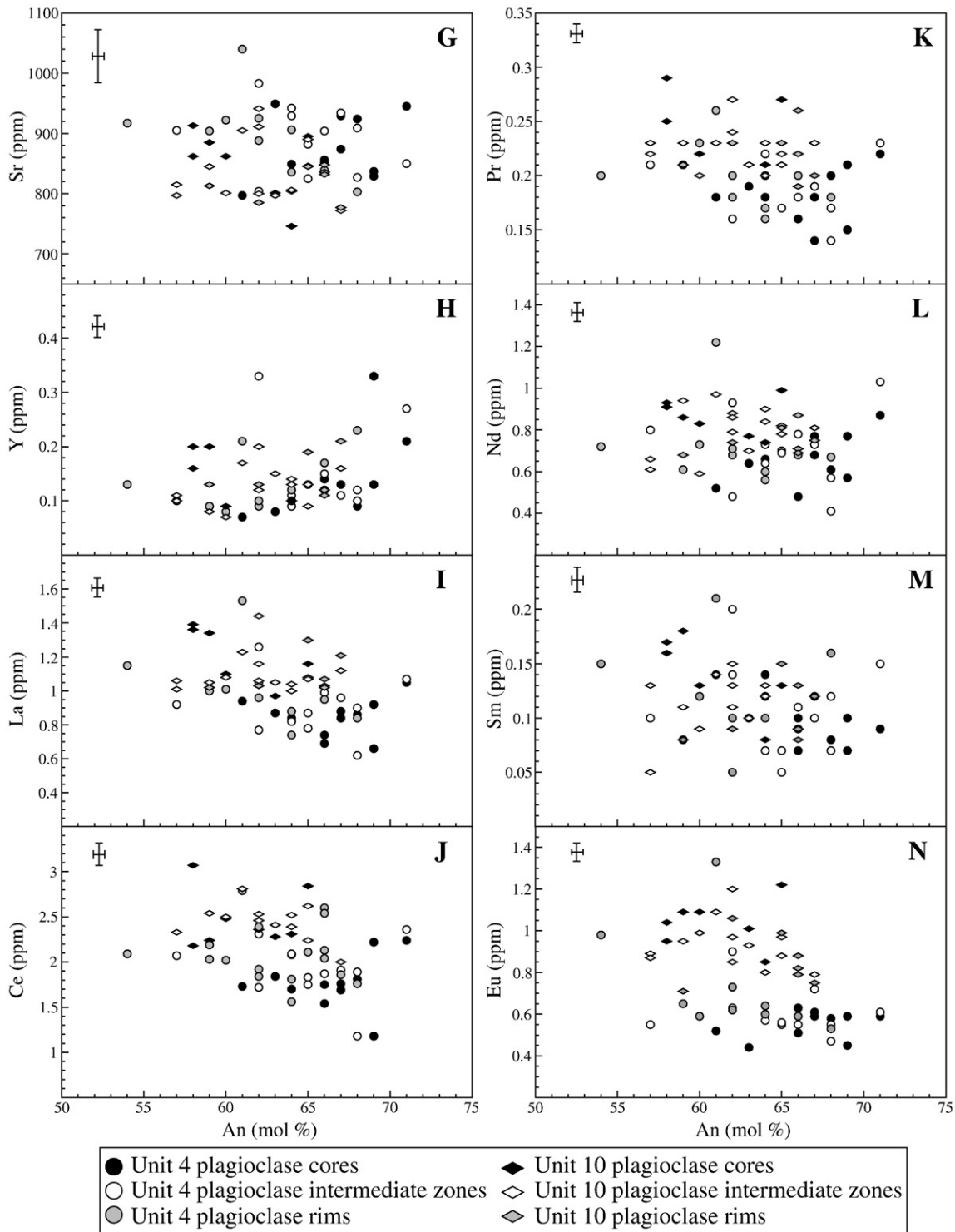


Fig. 9 (continued).

An interesting feature is apparent when the $^{87}\text{Sr}/^{86}\text{Sr}_i$ range of Unit 10 plagioclase zones are compared (Fig. 10). Unit 10 crystal zones have overlapping $^{87}\text{Sr}/^{86}\text{Sr}_i$, but rims trend to the lowest values and interiors (intermediate and core zones) have the highest $^{87}\text{Sr}/^{86}\text{Sr}_i$ values measured in Unit 10 crystals. A majority of Unit 10 crystals exhibit reverse zonation, which implies that the parent magmas of Unit 10 crystal rims were overall not only hotter but also more primitive in terms of composition relative to parent magmas of crystal interiors. Unit 10 plagioclase Sr isotope data imply that initial Unit 10

plagioclase growth occurred in magma that had already assimilated continental crust, then experienced growth from a somewhat less contaminated magma just prior to or during eruption.

5.4. Insights from trace elements and inverted parent magma compositions

Plagioclase parent magmas from Units 4 and 10 overlap whole-rock fields defined by published data (Ingle et al., 2002b) for Site 1137

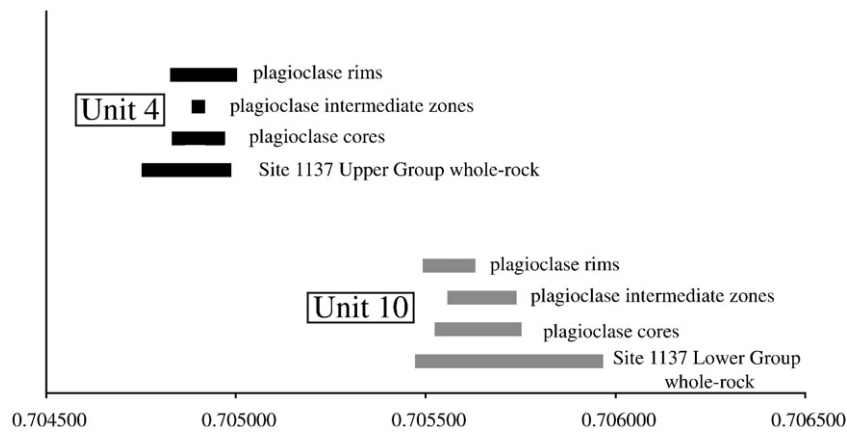


Fig. 10. The range of $^{87}\text{Sr}/^{86}\text{Sr}_1$ of Unit 4 and Unit 10 phenocrysts are shown relative to their respective host basalt whole-rock groups as defined by Ingle et al. (2002b). Note that plagioclase phenocrysts from each unit are similar to whole-rock $^{87}\text{Sr}/^{86}\text{Sr}_1$ reported by Ingle et al. (2002b). Unit 10 plagioclase rims are less radiogenic but still overlap intermediate and rim zones.

upper and lower basalt groups in Ba/Sr versus Rb space (Fig. 11A). This compositional overlap is consistent with Sr isotope similarities between Unit 4 and 10 basalts and their respective plagioclase phenocrysts, and provide further evidence that the phenocrysts record growth in both contaminated (Unit 10) and relatively uncontaminated (Unit 4) magmas. Indeed, relative to Unit 4 plagioclase parent magmas, the inferred parent magmas of Unit 10 crystals exhibit greater abundances of trace elements rich in continental crust (e.g. Pb, Ti, Ba, Rb, La). With the exception of greater light REE abundances in a few rim parent magmas relative to parent magmas of crystal interiors, there is little compositional distinction between the parent magmas of different Unit 4 crystal zones. This supports Sr isotope evidence that Unit 4 plagioclase phenocrysts formed in compositionally buffered uncontaminated parent magma (s). In general, parent magmas of Unit 10 crystal rims have lower abundances of Ba, Rb, and light REE relative to parent magmas of

crystal interiors. This supports Sr isotope evidence that some Unit 10 crystals experienced growth from somewhat less crustally contaminated magmas (relative to crystal interiors) just prior to or during eruption.

Calculated plagioclase parent magmas of crystals from both basalts, however, trend to lower La/Sm relative to their respective host basalt groups (Fig. 11C), and inverted parent magma trace element and REE abundances are generally lower than those of Site 1137 upper and lower basalt groups (Tables 4 and 5) (Ingle et al., 2002b). Lower abundances of these elements could indicate that Unit 4 and 10 plagioclase crystals grew from magmas that were more depleted than their host basalts. This is unlikely given the Sr isotope results and the compositional overlap in Fig. 11A. An alternative origin for the low parent magma trace element abundances may be the use of inaccurate partition coefficients and/or trace element diffusion.

It is difficult to gauge the accuracy of calculated partition coefficients, but Bindeman et al. (1998) and Blundy and Wood (1991) pointed out that An content is a dominant factor that affects cation substitution in plagioclase and temperature has a minor effect. Although An variations and crystallization temperatures are accounted for in partition coefficient calculations, it is possible that other factors influenced the accuracy of calculated D values. For example, Ba and Sr D values are probably the best constrained because they have been the focus of more partitioning experiments at natural trace element levels relative to lower abundance elements like the REE e.g., (Bindeman et al., 1998; Blundy and Wood, 1991).

5.5. Diffusive redistribution of trace elements?

Cherniak (1994, 2003) noted that at magmatic temperatures divalent cations diffuse faster through the plagioclase structure than trivalent cations. Cherniak (1994, 2003) also noted that diffusion occurs slower in An-rich plagioclase. Given the intermediate An contents ($\sim\text{An}_{54-71}$) of crystals examined in this study, the possibility of trace element re-distribution via diffusion warrants consideration. Zellmer et al. (1999) devised a simple test for diffusive equilibrium, which as they noted does not lead to a flat compositional profile, but rather a profile that mirrors the variation in trace element D values most heavily influenced by An content. Our Eq. (3) is an adaptation of Eq. (2) of Zellmer et al. (1999) that describes partitioning of a trace element (i) between plagioclase compositions A and B. When diffusive equilibrium has been reached between two adjacent plagioclase zones with An contents A and B the condition in Eq. (4) is met. This test was applied to each plagioclase crystal examined in this study for Sr and La at texturally distinct transitions between intermediate zones and crystal rims (Fig. 12). In the case of Unit 4 crystal P, where an intermediate zone to

Table 3
Unit 4 and 10 $^{87}\text{Sr}/^{86}\text{Sr}$ data.

Sample	Zone ^a	$^{87}\text{Sr}/^{86}\text{Sr}_M^b$	Rb/Sr ^c	$^{87}\text{Sr}/^{86}\text{Sr}_1^d$
<i>Site 1137 Unit 4 plagioclase</i>				
4-J	C rep1	0.704940 (12)	–	0.704939
4-J	C rep2	0.704965 (14)	–	0.704964
4-J	C avg	0.704953 (13)	0.0003	0.704950
4-J	I	0.704903 (10)	0.0003	0.704902
4-D	C	0.704850 (12)	0.0002	0.704849
4-D	R	0.704987 (68)	0.0004	0.704985
4-A	C rep1	0.704941 (12)	–	0.704939
4-A	C rep2	0.704936 (8)	–	0.704934
4-A	C avg	0.704939 (10)	0.0004	0.704937
4-A	R	0.704847 (6)	0.0004	0.704845
<i>Site 1137 Unit 10 plagioclase</i>				
10-1C-A	C	0.705738 (10)	0.0008	0.705735
10-1C-A	I	0.705725 (8)	0.0007	0.705722
10-1C-A	I	0.705689 (6)	0.0009	0.705685
10-2A-D	C	0.705575 (10)	0.0007	0.705572
10-2A-D	R	0.705513 (8)	0.0006	0.705510
10-2A-C	C	0.705545 (8)	0.0008	0.705542
10-1C-D	I	0.705577 (10)	0.0009	0.705575
10-1C-D	I	0.705623 (10)	0.0010	0.705620
10-1D-A	I	0.705640 (12)	0.0010	0.705637
10-1D-A	R	0.705539 (8)	0.0006	0.705536

^a C = core, I = intermediate zone, R = rim.

^b Values in parentheses are errors reported as measured 2σ in the last two decimal places of $^{87}\text{Sr}/^{86}\text{Sr}_M$.

^c Rb/Sr measured at coincident microdrill site by LA-ICP-MS.

^d A 107.7 Ma age of Site 1137 basalts from Duncan (2002) was used to correct Sr isotope ratios for in-situ decay. I subscript denotes initial $^{87}\text{Sr}/^{86}\text{Sr}$ ratio.

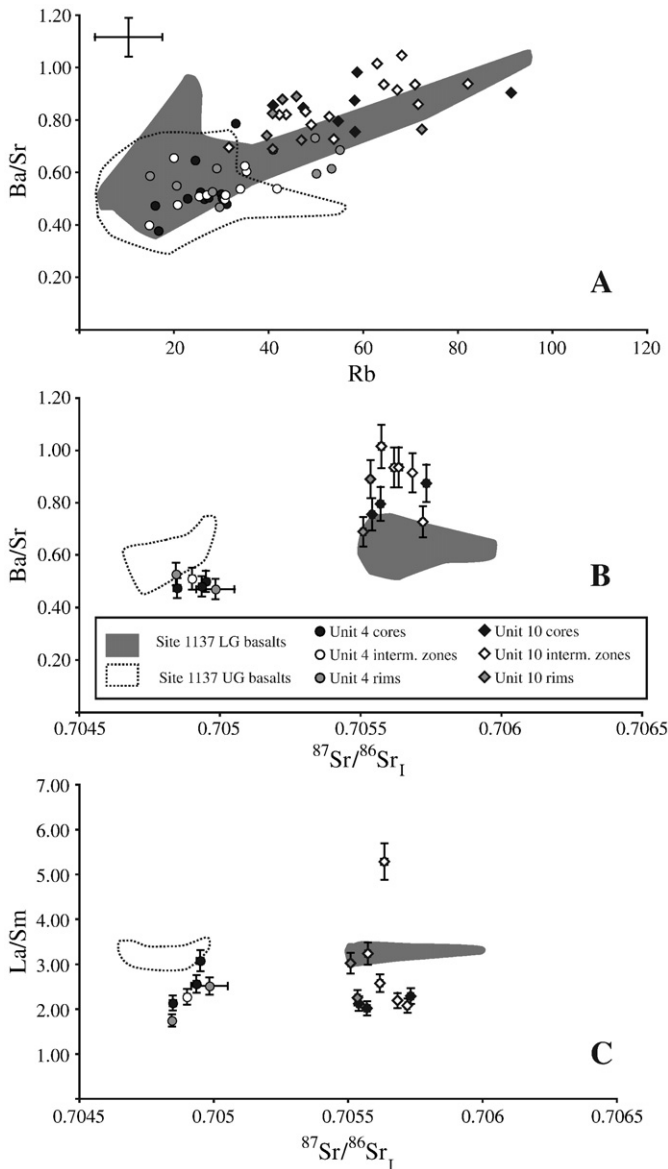


Fig. 11. A) Inverted Unit 4 and 10 plagioclase parent magmas (Tables 4, 5) overlap fields defined by whole-rock data for Site 1137 upper and lower group basalts. B) Inverted Unit 4 and 10 plagioclase parent magma Ba/Sr versus $^{87}\text{Sr}/^{86}\text{Sr}_I$ and Site 1137 basalt fields drawn using whole-rock data. C) Inverted Unit 4 and 10 plagioclase parent magma La/Sm versus $^{87}\text{Sr}/^{86}\text{Sr}_I$ and Site 1137 basalt fields drawn using whole-rock data reported by Ingle et al. (2002a). Plagioclase parent magma compositions overlap whole-rock basalt field in terms of $^{87}\text{Sr}/^{86}\text{Sr}_I$ but fall below or above whole-rock fields. The origin of this discrepancy is discussed in the text. Error bars represent measured 2σ error.

rim transition examination was not possible, a core-intermediate zone transition was tested. The partition coefficient values listed in Tables 4 and 5 were used for the test.

$$D_i^{A/B} = C_i^A / C_i^B = D_i^A / D_i^B \quad (3)$$

$$C_i^{A/B} / D_i^{A/B} = 1. \quad (4)$$

Two of the ten Unit 4 crystals (Q and P) are within error of the Sr diffusive equilibrium line (Eq. (4); Fig. 12A), whereas only one Unit 4 crystal (P) is within error of the La diffusive equilibrium line (Fig. 12C). Six of the seven Unit 10 crystals are within error of the Sr diffusive equilibrium line (Fig. 12B), whereas five of the seven crystals are within error of the La diffusive equilibrium line (Fig. 12D). These

observations are consistent with the findings of Cherniak (2003) that trivalent REE diffuse slower in plagioclase than divalent cations like Sr. Based upon these results, it is probable that trace element redistribution via diffusion is at least partially responsible for the lower than expected trace element abundances in reconstructed parent magmas. Strontium and La diffusion data also indicate that while the Unit 4 basalt has a higher modal abundance of plagioclase phenocrysts relative to Unit 10, the Unit 4 basalt contains a smaller proportion of phenocrysts held at magmatic temperatures for extended time. Simply put, the Unit 4 magma entrained more debris from more areas in its transit through the magma system than did the Unit 10 magma.

5.6. Magma ascent, incorporation of crystal debris, and compositional consequences

The texture and composition of a basalt is linked to the vigor and duration of the magmatic flux surrounding eruption, which means that a vigorous and long flux of primitive magma will lead to greater entrainment of crystal debris and extrusion of basalts with bulk-rock compositions that appear more primitive (Marsh, 2004). A batch of magma that must pass through large and/or numerous magma chambers may experience more compositional and textural buffering before arriving at the surface (Marsh, 1996). For example, vigorous ascent of primitive magma along the Y–Y' path in Fig. 13 would lead to eruption of a basalt with higher MgO and a greater abundance of phenocrysts relative to magma with a similar ascent rate along the path X–X', where magmas pass through a greater number of sills and chambers (Fig. 13). Magma ascent along Y–Y' in the magma system depicted in Fig. 13 proceeds via a feeder dike propagated along an existing plane of weakness in the surrounding rock, which can greatly enhance the rate at which a batch of magma ascends through the crust. The thermal structure of the crust also influences the nature of magma movement through the crust, where a higher thermal gradient leads to depressed magma cooling rates allowing greater volumes of magma to reach the surface (Sakimoto and Zuber, 1995).

We suggest that Unit 4 magmas ascended to the surface along a pathway similar to Y–Y', and Unit 10 magmas followed a pathway similar to X–X' (Fig. 13). Unit 4 and 10 bulk-rock data reported by Ingle et al. (2002b) and our petrographic observations support this hypothesis. Unit 4 basalts have higher MgO (5.8–7.1 wt.%) and greater plagioclase modal abundances than Unit 10 basalts (4.5–4.9 wt.% MgO) (Ingle et al., 2002b). Based upon downhole stratigraphy at Site 1137 (Fig. 2), by the time the Unit 4 basalt was erupted, recurring magmatism and volcanism likely altered the thermal structure of Elan Bank crust. Hotter Elan Bank crust may thus have been partially responsible for the more vigorous eruptive flux of the Unit 4 basalt relative to the older Unit 10 basalt. The notion that the Unit 4 and 10 basalts were erupted from the separate volcanic vents via different magma plumbing routes, as depicted in Fig. 13 is not certain. The Unit 4 and 10 basalts could indeed have the textures and compositions that they possess and still have been erupted from the same vent via the same plumbing system. That the plagioclase-rich debris incorporated into each basalt has distinct Sr isotope ratios and trace element compositions indicates that they likely did not originate from the same vent and magma plumbing route. Simply put, the Unit 4 and 10 basalts do not appear to have picked up their phenocrysts from the same piles of plagioclase-rich debris. After eruption of the Unit 10 basalt and prior to emplacement of the Unit 4 basalt, deposits of sandstone, fluvial conglomerate, and more evolved volcanoclastic rocks were laid down. Given the spacing in time between their emplacements, it is quite plausible that these two basalts arrived at the surface via different routes through the KP magma system as depicted in Fig. 13.

Abundant evidence of plagioclase remobilization and resorption during magma recharge highlights the possibility that the bulk-rock isotopic signature can be influenced by the isotopic signature of the entrained plagioclase-rich debris. Such entrainment may serve to

Table 4
Unit 4 plagioclase partition coefficients and inferred parent magma compositions 1=zone; 2=An (Mol%).

Sample	Zone	An (mol%)	D_{Rb}	D_{Sr}	D_Y	D_{Ba}	D_{La}	D_{Ce}	D_{Pr}	D_{Nd}	D_{Sm}	Rb	Sr	Y	Ba	La	Ce	Pr	Nd	Sm
4-K	C	69	0.01	1.77	0.01	0.27	0.10	0.09	0.07	0.05	0.03	33.1	467.4	39.4	367.3	8.8	25.6	3.0	14.3	2.2
4-K	I	71	0.01	1.70	0.01	0.25	0.10	0.09	0.07	0.05	0.03	20.0	499.7	31.9	327.6	10.4	27.3	3.3	18.9	4.8
4-K	R	66	0.01	1.86	0.01	0.30	0.10	0.09	0.07	0.05	0.03	14.9	452.1	19.9	265.2	9.1	23.5	2.8	12.8	3.0
4-L	C	61	0.01	2.00	0.01	0.35	0.11	0.09	0.07	0.05	0.03	25.6	397.6	8.2	208.4	8.8	19.9	2.6	10.0	4.9
4-L	I	62	0.01	1.98	0.01	0.34	0.11	0.09	0.07	0.05	0.03	35.3	405.3	38.0	244.8	7.3	19.8	2.4	9.3	4.9
4-L	R	68	0.01	1.79	0.01	0.28	0.10	0.09	0.07	0.05	0.03	20.6	448.0	26.5	246.0	8.0	20.3	2.6	12.4	5.0
4-Q	C	66	0.01	1.85	0.01	0.29	0.10	0.09	0.07	0.05	0.03	30.0	461.2	13.6	238.6	7.1	20.1	2.3	9.0	3.3
4-Q	I	65	0.01	1.89	0.01	0.31	0.11	0.09	0.07	0.05	0.03	20.8	465.9	15.4	221.7	8.3	21.1	2.5	13.3	1.6
4-Q	R	60	0.01	2.02	0.01	0.36	0.11	0.09	0.07	0.05	0.03	0.0	456.4	8.8	254.1	9.5	23.2	3.4	14.1	4.0
4-P	C	66	0.01	1.85	0.01	0.29	0.10	0.09	0.07	0.05	0.03	30.2	463.2	16.1	232.0	6.6	17.7	2.3	9.0	2.4
4-P	I	65	0.01	1.90	0.01	0.31	0.11	0.09	0.07	0.05	0.03	30.7	435.2	14.8	216.3	7.4	20.1	2.4	13.1	2.4
4-J	C	68	0.01	1.79	0.01	0.28	0.10	0.09	0.07	0.05	0.03	26.4	515.8	10.3	256.8	8.3	20.9	2.8	11.3	2.7
4-J	I	68	0.01	1.81	0.01	0.28	0.10	0.09	0.07	0.05	0.03	25.4	502.8	11.6	255.6	8.6	21.8	2.5	10.6	3.8
4-J	R	62	0.01	1.98	0.01	0.34	0.11	0.09	0.07	0.05	0.03	29.0	468.2	10.3	288.0	9.9	22.1	2.9	13.0	1.8
4-N	C	64	0.01	1.90	0.01	0.31	0.11	0.09	0.07	0.05	0.03	22.9	446.4	11.8	223.1	8.0	19.6	2.6	12.5	4.5
4-N	R	61	0.01	1.99	0.01	0.34	0.11	0.09	0.07	0.05	0.03	49.8	523.2	23.8	382.6	14.4	32.1	3.8	23.4	7.1
4-O	C	67	0.01	1.83	0.01	0.29	0.10	0.09	0.07	0.05	0.03	27.3	478.7	15.2	240.9	8.1	20.3	2.1	12.6	3.3
4-O	I	67	0.01	1.83	0.01	0.29	0.10	0.09	0.07	0.05	0.03	35.0	509.5	12.3	318.2	9.2	22.0	2.8	13.7	3.1
4-O	I	57	0.01	2.12	0.01	0.40	0.11	0.09	0.07	0.05	0.03	41.8	426.6	11.0	229.6	8.6	23.9	3.1	15.7	3.4
4-O	I	62	0.01	1.97	0.01	0.34	0.11	0.09	0.07	0.05	0.03	40.9	498.4	11.3	342.0	11.9	26.6	2.9	17.8	6.9
4-O	R	54	0.01	2.23	0.01	0.44	0.11	0.09	0.07	0.05	0.03	55.1	411.6	14.8	282.2	10.7	24.2	3.0	14.4	5.6
4-D	C	67	0.01	1.82	0.01	0.28	0.10	0.09	0.07	0.05	0.03	16.0	510.6	14.8	241.2	8.4	19.5	2.6	14.4	3.9
4-D	R	64	0.01	1.93	0.01	0.32	0.11	0.09	0.07	0.05	0.03	29.6	470.3	13.4	220.0	8.4	17.9	2.4	10.6	3.3
4-A	C	63	0.01	1.95	0.01	0.33	0.11	0.09	0.07	0.05	0.03	31.1	485.4	9.3	232.3	8.2	21.2	2.7	12.1	3.2
4-A	I	64	0.01	1.93	0.01	0.32	0.11	0.09	0.07	0.05	0.03	34.0	482.2	10.4	259.1	7.8	23.9	2.9	12.2	2.4
4-A	I	64	0.01	1.92	0.01	0.32	0.11	0.09	0.07	0.05	0.03	30.9	491.7	13.2	252.5	8.3	24.0	3.2	13.8	3.3
4-A	R	64	0.01	1.91	0.01	0.32	0.11	0.09	0.07	0.05	0.03	28.2	437.0	11.9	229.7	7.0	20.8	2.2	11.4	4.0
4-C	C	71	0.01	1.70	0.01	0.25	0.10	0.09	0.07	0.05	0.03	24.5	554.3	24.5	357.9	10.2	25.9	3.1	16.1	2.8
4-C	I	66	0.01	1.85	0.01	0.30	0.10	0.09	0.07	0.05	0.03	27.0	487.4	17.0	250.3	9.4	21.5	2.6	14.6	3.6
4-C	R	59	0.01	2.06	0.01	0.37	0.11	0.09	0.07	0.05	0.03	50.1	439.3	9.9	261.6	9.4	23.4	3.1	11.9	2.6

¹C = core; I = intermediate zone; R = rim.

²[An = Ca / (Ca + Na + K)] * 100.

either dilute or enrich the isotopic signature of the whole-rock. For example, Unit 4 plagioclase crystals bracket the more radiogenic end of the Unit 4 whole-rock Sr isotope range and extend to slightly higher ⁸⁷Sr/⁸⁶Sr₁ than any Site 1137 upper group whole-rock sample reported by Ingle et al. (2002b) (Fig. 10). It is quite possible that crystals bearing

Sr isotope signatures considerably more enriched than Unit 4 basalts exist and were missed via our relatively limited sampling of ten Unit 4 crystals. If the Unit 4 basalt examined in this study had incorporated more plagioclase-rich debris, it indeed might have had a bulk-rock composition reflecting minor crustal contamination.

Table 5
Unit 10 plagioclase partition coefficients and inferred parent magma compositions 1=zone; 2=An (Mol%).

Sample	Zone	An (mol%)	D_{Rb}	D_{Sr}	D_Y	D_{Ba}	D_{La}	D_{Ce}	D_{Pr}	D_{Nd}	D_{Sm}	Rb	Sr	Y	Ba	La	Ce	Pr	Nd	Sm
10-1C-A	C	60	0.01	2.02	0.01	0.36	0.11	0.09	0.07	0.05	0.03	58.3	426.8	10.3	372.3	10.3	28.5	3.2	16	4.5
10-1C-A	I	65	0.01	1.90	0.01	0.31	0.11	0.09	0.07	0.05	0.03	53.9	469.3	14.5	340.4	10.3	25.8	3.0	14.8	5.0
10-1C-A	I	62	0.01	1.96	0.01	0.33	0.11	0.09	0.07	0.05	0.03	67.3	464.7	13.9	424.3	11.0	29.1	3.5	16.7	5.0
10-1C-A	R	66	0.01	1.86	0.01	0.30	0.10	0.09	0.07	0.05	0.03	47.0	449.3	14.1	324.2	9.8	24.5	2.8	13.4	2.7
10-1C-B1	C	65	0.01	1.87	0.01	0.30	0.11	0.09	0.07	0.05	0.03	58.8	478.1	14.8	468.9	11.0	32.7	3.9	18.6	4.3
10-1C-B1	I	61	0.01	1.99	0.01	0.35	0.11	0.09	0.07	0.05	0.03	82.2	455.2	19.6	426.0	11.6	32.3	3.3	18.6	4.7
10-1C-B1	I	65	0.01	1.87	0.01	0.30	0.11	0.09	0.07	0.05	0.03	43.8	452.4	10.9	370.8	10.2	30.1	3.2	15.4	5.0
10-1C-B1	I	64	0.01	1.90	0.01	0.31	0.11	0.09	0.07	0.05	0.03	47.9	422.7	16.2	351.0	9.5	27.5	2.9	16.0	4.3
10-1C-B1	R	66	0.01	1.84	0.01	0.29	0.10	0.09	0.07	0.05	0.03	40.9	460.0	12.4	378.9	10.2	29.9	3.2	16.4	2.8
10-1C-B2	C	58	0.01	2.08	0.01	0.38	0.11	0.09	0.07	0.05	0.03	91.4	438.6	22.5	395.9	13.0	35.4	4.2	17.9	5.4
10-1C-B2	I	64	0.01	1.92	0.01	0.32	0.11	0.09	0.07	0.05	0.03	49.1	419.1	14.8	327.0	9.9	29.0	3.3	17.1	3.9
10-1C-B2	I	62	0.01	1.98	0.01	0.34	0.11	0.09	0.07	0.05	0.03	42.4	404.2	14.5	330.6	10.0	28.3	3.3	15.1	3.9
10-1C-B2	R	59	0.01	2.07	0.01	0.38	0.11	0.09	0.07	0.05	0.03	72.5	392.3	14.1	299.2	9.6	25.2	3.1	13.2	2.9
10-2A-D	C	59	0.01	2.06	0.01	0.37	0.11	0.09	0.07	0.05	0.03	54.8	430.1	22.3	341.5	12.6	25.8	3.4	16.8	6.3
10-2A-D	R	67	0.01	1.84	0.01	0.29	0.10	0.09	0.07	0.05	0.03	41.0	422.8	24.6	290.8	11.6	21.4	2.8	14.0	3.8
10-2A-C	C	58	0.01	2.10	0.01	0.39	0.11	0.09	0.07	0.05	0.03	58.4	411.2	18.5	309.7	12.7	25.1	3.6	18.2	6.0
10-2A-C	I	62	0.01	1.97	0.01	0.34	0.11	0.09	0.07	0.05	0.03	71.7	476.8	22.3	409.2	13.6	27.1	3.9	16.4	4.4
10-2A-C	I	67	0.01	1.82	0.01	0.29	0.10	0.09	0.07	0.05	0.03	31.7	423.5	18.6	293.8	10.7	23.0	3.3	15.1	4.0
10-2A-C	R	65	0.01	1.87	0.01	0.30	0.11	0.09	0.07	0.05	0.03	39.7	451.6	21.5	333.9	12.4	24.3	3.4	15.2	5.0
10-1C-D	C	63	0.01	1.94	0.01	0.33	0.11	0.09	0.07	0.05	0.03	47.4	413.4	17.0	349.3	9.1	26.2	3.0	14.6	3.3
10-1C-D	I	60	0.01	2.05	0.01	0.37	0.11	0.09	0.07	0.05	0.03	63.0	391.0	7.7	396.3	10.1	28.8	2.9	11.4	3.1
10-1C-D	I	63	0.01	1.95	0.01	0.33	0.11	0.09	0.07	0.05	0.03	68.2	409.4	16.9	427.6	9.9	27.7	3.1	13.3	3.3
10-1C-D	I	59	0.01	2.06	0.01	0.37	0.11	0.09	0.07	0.05	0.03	71.0	409.6	9.5	382.2	9.8	29.3	3.4	18.2	3.8
10-1C-D	R	62	0.01	1.98	0.01	0.34	0.11	0.09	0.07	0.05	0.03	43.0	396.3	15.0	347.7	9.7	27.5	3.3	14.1	3.0
10-1D-A	I	57	0.01	2.12	0.01	0.40	0.11	0.09	0.07	0.05	0.03	52.9	376.3	12.6	305.4	9.9	26.9	3.2	12.0	4.6
10-1D-A	I	57	0.01	2.11	0.01	0.39	0.11	0.09	0.07	0.05	0.03	64.4	385.6	11.5	359.9	9.4	26.9	3.4	13.0	1.8
10-1D-A	R	66	0.01	1.85	0.01	0.30	0.10	0.09	0.07	0.05	0.03	46.0	449.6	12.4	399.5	9.7	29.2	3.7	12.9	4.3

¹C = core; I = intermediate zone; R = rim.

²[An = Ca / (Ca + Na + K)] * 100.

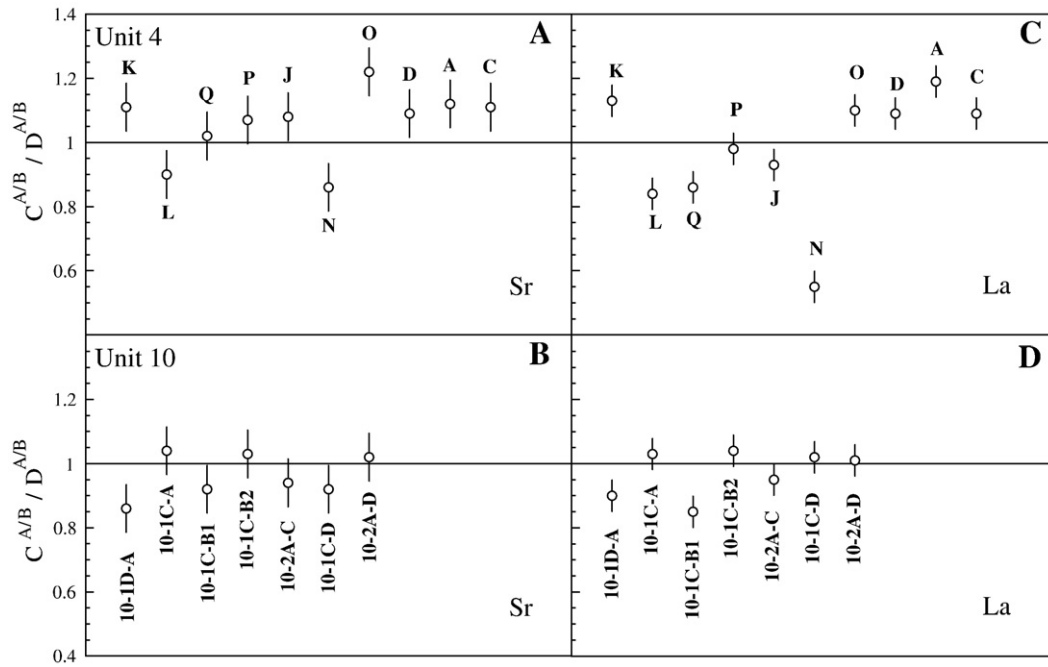


Fig. 12. Extents of diffusive equilibrium for (from Eq. (4)) for Unit 4 and 10 plagioclase crystals. A) Two of ten Unit 4 crystals are within analytical uncertainty (the propagated 2σ error when values are divided, e.g., Sr/Sr) of having reached Sr diffusive equilibrium, whereas one of ten have reached La diffusive equilibrium. C) The diffusive equilibrium line is drawn based upon Eq. (4). B) Six of seven Unit 10 phenocrysts are within error of having reached Sr diffusive equilibrium, whereas five of seven crystals are within error of the La diffusive equilibrium line. These results are consistent with the findings of Cherniak (2003) that La diffuses more slowly than Sr in plagioclase.

5.7. Plagioclase phenocrysts, glomerocrysts and the KP magma system at Elan Bank

Mantle derived magmas from the Kerguelen hotspot ascended through the Indian Ocean lithosphere and in some cases interacted

with stranded fragments of continental crust en route to the surface (Frey et al., 2000). The architecture of the magma chamber system beneath Elan Bank and the physical manner in which crustal rocks were assimilated are not strictly known, but it is clear from our observations that crustal assimilation pre-dated the formation of the

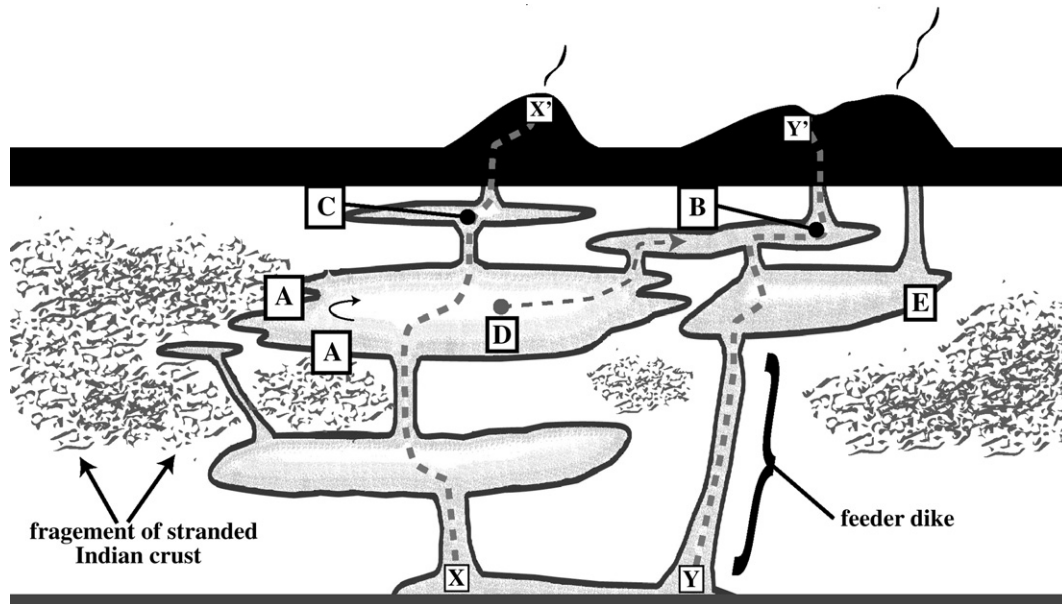


Fig. 13. A simplified schematic of the magma system beneath Elan Bank. Crustal contamination occurred before formation of plagioclase phenocrysts, where expansion of newly formed sills and conduits eroded into stranded fragments of continental crust at the points labeled A. Shallow crystallization of plagioclase and/or sorting of crystals via repeated movement of magma over time lead points B, C and E to be dominated by plagioclase-rich debris. The eruptions that brought the Unit 4 and 10 basalts tapped the sills labeled B and C, respectively. Crystals grown in chambers that contacted stranded crustal rocks may have transported crystals + liquid to uncontaminated portions of the system as depicted by the pathway labeled D. We suggest Unit 10 magmas passed through the Elan Bank magma chamber system along a path similar to X–X', which accounts for their crustally contaminated signatures and evidence of a less vigorous eruptive flux. We suggest that Unit 4 magmas followed a more direct route to the surface via passage through fewer sills and conduits. Unit 4 magmas passed through a section of the magma system that was either not in contact with stranded crust or was well armored immediately after contamination as depicted by the path Y–Y'. Crystals with Sr isotope signatures more radiogenic than Unit 4 bulk-rock samples may have originated via path D.

plagioclase phenocrysts hosted in the Unit 4 and 10 basalts. Plagioclase-rich debris was common in the section of the magma system tapped when the Unit 4 and 10 basalts were erupted. Understanding the origin of this debris within the magma system is thus key to understanding the information these crystals hold and the full petrogenetic history of Elan Bank basalts.

Clinopyroxene and olivine are notably absent within glomerocrysts and as dominant phenocryst phases in both basalts, one of which appears to have arrived at the surface via a vigorous eruptive flux (Unit 4). Clinopyroxene has a stability field that contracts at low pressure, and at low pressure plagioclase and olivine remain stable basaltic liquidus phases. The dominance of plagioclase and lack of clinopyroxene indicates that crystallization occurred at a relatively shallow depth in the Elan Bank crust. Alternatively, it is also possible that sorting of crystal debris occurred during subterranean magmatic flow at Elan Bank. The lack of significant olivine in these two basalts, particularly the Unit 4 basalt (MgO up to 7.1 wt.%), lends support to the notion that the plagioclase-rich debris piles were formed at least in part by flow sorting of crystals. Marsh (2004) cited evidence of kinetic sieving and flow sorting of plagioclase and orthopyroxene in the well exposed Ferrar dolerite magma chamber system and presented evidence that sorting of crystals progressed outward and upward from points of magma filing. It is conceivable that higher density clinopyroxene and olivine remained at depth, while less dense plagioclase cumulates dominated the shallow and lateral extensions of the Elan Bank magma chamber system (locations B, C, and E in Fig. 13). While it is not clear whether plagioclase-dominated crystallization or flow sorting of plagioclase are responsible for formation of the reservoir of plagioclase-rich debris, either mechanism can be reconciled to explain our observations.

Magma chambers are often modeled as simple bodies dominated by liquid that fractionate crystals to explain geochemical and petrographic observations (Sano and Yamashita, 2004), or as physically complex arrangements of interconnected dikes, sills, and conduits based upon seismic data (Ryan et al., 1981). The magmatic mush column model of Marsh (1996, 2004, 2006), which consists of a stack of interconnected sheets, sills, and conduits, reconciles the physical complexities of magma systems with the textures and compositions of their volcanic products. The mush column model is best illustrated by the Ferrar dolerites (Marsh, 2004). The Ferrar dolerites consist of a series of interconnected dikes and sills and a contiguous continental flood basalt (Kirkpatrick basalt) in the McMurdo Dry Valleys of Antarctica (Marsh, 2004). The Kirkpatrick basalt ascended through crust that was thinned due to rifting related to break up of Gondwana (Fleming et al., 1995; Marsh, 2004). The thermal structure of the Gondwanan crust was altered at this location due to rifting, which would have made ascent of greater volumes of magma possible. In a similar manner, magma ascending below Elan Bank encountered Gondwanan crust thermally perturbed by recurring magmatism. Vertically heterogeneous crust and zones of neutral buoyancy existed beneath both Elan Bank and in the Ferrar system (Ryan, 1987). Based upon these shared characteristics, it is quite plausible that Elan Bank magmas encountered a complex mush column magma system. Damasceno et al. (2002) suggested that basalts from a younger portion of the Kerguelen Plateau, the Mont Crozier section of the Kerguelen Archipelago, passed through a magmatic system that consisted of a complex arrangement of interconnected conduits and chambers. They also suggested that plagioclase-dominated partial crystallization occurred primarily in shallow sub-volcanic magma reservoirs (Damasceno et al., 2002).

6. Summary and conclusions

We suggest that Elan Bank magmas passed through a magmatic mush column type of magma system. An Elan Bank magmatic mush

column would have contained the types of plagioclase-rich debris zones that the Unit 4 and 10 basalts tapped during eruption. Progressive upward movement of magma and/or shallow level crystallization were the mechanisms for the formation of plagioclase-dominated environments at the locations labeled B, C, and E in Fig. 13. Locations B, C and E in Fig. 13 were the sections of the magma chamber system that were tapped during eruption of the Unit 4 and 10 basalts. We suggest that Unit 10 magmas ascended a section of the KP magma system that penetrated stranded continental crust (path X–X' in Fig. 13). Crustal assimilation occurred prior to formation of plagioclase phenocrysts. Intruding primitive KP magmas assimilated crust at points where sills and conduits grew laterally and vertically and penetrated into stranded crustal fragments (location A in Fig. 13). The period of greatest crustal assimilation surrounded the initial erosion of country rock as new sills and conduits were formed. Magma chamber walls became armored via inward growth of solidification fronts, which began to grow immediately after emplacement (Marsh, 1996). Crystals grown after sill emplacement, where sills intruded into fragments of stranded continental crust, bear signatures of crustally contamination. After armoring, new magma input likely stirred the crystals and liquid in the chamber interior, picked up and partially resorbed crystal debris, and carried some of the debris to shallower sections of the system (Marsh, 1996; Kuritani, 1998). This action repeated over time carried the crustal contamination signature throughout the system, which possibly included transport to sills that did not intrude crustal rocks (e.g., see path D in Fig. 13). We suggest Unit 4 magmas passed through a section of the KP magma system that did not significantly penetrate stranded continental crust (see path Y–Y' in Fig. 13). Relative to the Unit 10 eruption, the Unit 4 eruptive flux was stronger, which stirred up a wider variety of crystal debris. Despite the wider variety of phenocrysts, we observed little evidence of significant crustal contamination. We suggest that the sections of the KP magma system tapped during eruption of the Unit 4 basalt allowed magmas to ascend rapidly. This rapid ascent was likely related to an elevated thermal gradient within the crust and/or a vertically aligned plane of weakness that provided a pathway for rapid magma ascent.

Acknowledgments

This research used samples provided by the Ocean Drilling Program (ODP). ODP was sponsored by the US National Science Foundation and participating countries under management of the Joint Oceanographic Institutions. We are indebted to the staff and crew of the *RV JOIDES Resolution* whose professionalism and cooperation allowed the collection of drill cores at Site 1137. A special thanks to Prof. Gerhard Wörner for a thorough and tremendously useful review of this manuscript. Funding was provided to CRN by NSF for this work under OCE-0452102. Support from the University of Notre Dame to WSK is gratefully acknowledged. We also thank Prof. D. Graham Pearson, Dr. Geoff Nowell, Dr. Dan Morgan and Dr. Bruce Charlier for their direct and indirect efforts and support with this project.

References

- Asimow, P.D., Ghiorso, M.S., 1998. Algorithmic modifications extending MELTS to calculate subsolidus phase relations. *American Mineralogist* 83, 1127–1131.
- Bindeman, I.N., Davis, A.M., Drake, M.J., 1998. Ion microprobe study of plagioclase-basalt partition experiments at natural concentration levels in trace elements. *Geochimica et Cosmochimica Acta* 62 (7), 1175–1193.
- Blundy, J., 1997. Experimental study of a Kiglapait marginal rock and implications for trace element partitioning in layered intrusions. *Chemical Geology* 141, 73–92.
- Blundy, J.D., Wood, B.J., 1991. Crystal-chemical controls on the partitioning of Sr and Ba between plagioclase feldspar, silicate melts, and hydrothermal solutions. *Geochimica et Cosmochimica Acta* 55, 193–209.
- Blundy, J., Wood, B., 1994. Prediction of crystal-melt partition coefficients. *Nature* 372 (1), 452–454.
- Blundy, J.D., Wood, B.J., 2003. Partitioning of trace elements between crystals and melts. *Earth and Planetary Science Letters* 210, 383–397.

- Brice, J.C., 1975. Some thermodynamic aspects of the growth of strained crystals. *Journal of Crystal Growth* 28, 249–254.
- Charlier, B.L.A., Ginibre, C., Morgan, D., Nowell, G.M., Pearson, D.G., Davidson, J.P., Ottley, C.J., 2006. Methods for the microsampling and high-precision analysis of strontium and rubidium isotopes at single crystal scale for petrological and geochronological applications. *Chemical Geology* 232, 114–133.
- Cherniak, D.J., 1994. A study of strontium diffusion in plagioclase using Rutherford backscattering spectroscopy. *Geochimica et Cosmochimica Acta* 58, 5179–5190.
- Cherniak, D.J., 2003. REE diffusion in feldspar. *Chemical Geology* 193, 25–41.
- Coffin, M.F., Eldholm, O., 1993. Scratching the surface: estimating the dimensions of large igneous provinces. *Geology* 21, 515–518.
- Coffin, M.F., Eldholm, O., 1994. Large igneous provinces: crustal structure, dimensions, and external consequences. *Reviews of Geophysics* 32, 1–36.
- Damasceno, D., Scoates, J.S., Weis, D., Frey, F.A., Giret, A., 2002. Mineral chemistry of mildly alkalic basalts from the 25 Ma Mont. Crozier Section, Kerguelen Archipelago: constraints on phenocryst crystallization environments. *Journal of Petrology* 43 (7), 1389–1413.
- Davidson, J.P., Hora, J.M., Garrison, J.M., Dungan, M.A., 2005. Crustal forensics in arc magmas. *Journal of Volcanology and Geothermal Research* 140, 157–170.
- Duncan, R., 2002. A time frame for construction of the Kerguelen Plateau and Broken Ridge. *Journal of Petrology* 43 (7), 1109–1119.
- Eggins, S.M., Shelley, J.M.G., 2002. Compositional heterogeneity in NIST SRM 610–617 glasses. *Geostandards Newsletter* 26 (3), 269–286.
- Fleming, T.H., Foland, K.A., Elliott, D.H., 1995. Isotopic and chemical constraints on the crustal evolution and source signature of Ferrar magmas, North Victoria Land, Antarctica. *Contributions to Mineralogy and Petrology* 121, 217–236.
- Font, I., Nowell, G.M., Pearson, D.G., Ottley, C.J., Willis, S.G., 2007. Sr isotope analysis of bird feathers by TIMS: a tool to trace bird migration paths and breeding sites. *Journal of Analytical Atomic Spectrometry* 22, 513–522.
- Frey, F.A., Coffin, M.F., Wallace, P.J., Weis, D., Zhao, X., Wise, S.W., Wähnert, V., Teagle, D.A.H., Saccoccia, P.J., Reusch, D.N., Pringle, M.S., Nicolaysen, K.E., Neal, C.R., Müller, R.D., Moore, C.L., Mahoney, J.J., Keszthelyi, L., Inokuchi, H., Duncan, R.A., Delius, H., Damuth, J.E., Damasceno, D., Coxal, H.K., Borre, M.K., Boehm, F., Barling, J., Arndt, N.T., Antretter, M., 2000. Origin and evolution of a submarine large igneous province: the Kerguelen Plateau and Broken Ridge, southern Indian Ocean. *Earth and Planetary Science Letters* 176, 73–89.
- Frey, F.A., Weis, D., Borisova, A.Y., Xu, G., 2002. Involvement of continental crust in the formation of the Cretaceous Kerguelen Plateau: new perspectives from ODP Leg 120 Sites. *Journal of Petrology* 43 (7), 1207–1239.
- Ghiorso, M., Sack, R., 1995. Chemical mass transfer in magmatic processes. IV. A revised internally consistent thermodynamic model for interpolation and extrapolation of liquid–solid equilibria in magmatic systems at elevated temperatures and pressure. *Contributions to Mineralogy and Petrology* 119, 197–212.
- Ginibre, C., Wörner, G., Kronz, A., 2002. Minor- and trace-element zoning in plagioclase: implications for magma chamber processes at Parícutin volcano, northern Chile. *Contributions to Mineralogy and Petrology* 143, 300–315.
- Ingle, S., Weis, D., Frey, F., 2002a. Indian continental crust recovered from Elan Bank, Kerguelen Plateau (ODP Leg 183, Site 1137). *Journal of Petrology* 43, 1241–1257.
- Ingle, S., Weis, D., Scoates, J., Frey, F.A., 2002b. Relationship between the early Kerguelen plume and continental flood basalts of the paleo-Eastern Gondwanan margins. *Earth and Planetary Science Letters* 197, 35–50.
- Kent, R.W., Pringle, M.S., Saunders, A.D., Ghose, N.C., 2001. $^{40}\text{Ar}/^{39}\text{Ar}$ age of the Rajmahal basalts, India, and their relationship to the southern Kerguelen Plateau. *Journal of Petrology* 43, 1141–1153.
- Kinman, W.S., Neal, C.R., 2006. Magma evolution revealed by anorthite-rich plagioclase cumulate xenoliths from the Ontong Java Plateau: insights into magma dynamics and melt evolution. *Journal of Volcanology and Geothermal Research* 154, 131–157.
- Kuritani, T., 1998. Boundary layer crystallization in a basaltic magma chamber: evidence from Rishiri Volcano, Northern Japan. *Journal of Petrology* 39, 1619–1640.
- Langmuir, C.H., 1989. Geochemical consequences of in situ crystallization. *Nature* 340, 199–205.
- Longerich, H.P., 1996. Laser ablation inductively coupled plasma mass spectrometric transient signal data acquisition and analyte concentration calculation. *Journal of Analytical Atomic Spectrometry* 11, 899–904.
- Mahoney, J.J., Jones, W.B., Frey, F.A., Salters, V.J.M., Pyle, D.G., Davies, H.L., 1995. Geochemical characteristics of lavas from Broken Ridge, the Naturaliste Plateau and southernmost Kerguelen Plateau: Cretaceous plateau volcanism in the southeast Indian Ocean. *Chemical Geology* 120, 315–345.
- Marsh, B., 1996. Solidification fronts and magma dynamics. *Mineralogical Magazine* 60, 5–40.
- Marsh, B., 2004. A Magmatic Mush Column Rosetta Stone: the McMurdo Dry Valleys of Antarctica. *Eos, Transactions — American Geophysical Union* 85 (47), 497–502.
- Marsh, B., 2006. Dynamics of magma chambers. *Elements* 2, 287–292.
- Neal, C.R., Mahoney, J.J., Chazey, W.J., 2002. Mantle sources and the highly variable role of continental lithosphere in basalt petrogenesis of the Kerguelen Plateau and Broken Ridge LIP: results from ODP Leg 183. *Journal of Petrology* 43 (7), 1177–1205.
- Nicolaysen, K., Bowring, S., Frey, F.A., Weis, D., Ingle, S., Pringle, M.S., Coffin, M.F., Leg 183 Shipboard Scientific Party, 2001. Provenance of Proterozoic garnet–biotite gneiss recovered from Elan Bank, Kerguelen Plateau, southern Indian Ocean. *Geology* 29, 235–238.
- Operto, S., Charvis, P., 1996. Deep structure of the southern Kerguelen Plateau (southern Indian Ocean) from ocean bottom seismometer wide-angle seismic data. *Journal of Geophysical Research* 101 (B11), 25077–25103.
- Ryan, M.P., 1987. Neutral buoyancy and the mechanical evolution of magmatic systems. In: Mysen, B.O. (Ed.), *Magmatic Processes: Physicochemical Principles*. The Geochemical Society Special Publication, vol. 1, pp. 259–288.
- Ryan, M.P., Koyanagi, R.Y., Fiske, R.S., 1981. Modeling the three-dimensional structure of macroscopic magma transport systems: application to Kilauea Volcano, Hawaii. *Journal of Geophysical Research* 86, 7111–7129.
- Sakimoto, S.E.H., Zuber, M.T., 1995. Effects of planetary thermal structure on the ascent and cooling of magma on Venus. *Journal of Volcanology and Geothermal Research* 64, 53–60.
- Sano, T., Yamashita, S., 2004. Experimental petrology of basement lavas from Ocean Drilling Program Leg 192: implications for differentiation processes in Ontong Java Plateau magmas. In: Fitton, J.G., Mahoney, J.J., Wallace, P.J., Saunders, A.D. (Eds.), *Origin and Evolution of the Ontong Java Plateau*. Geological Society, Special Publications, London, vol. 229, pp. 185–218.
- Saunders, A., Storey, M., Gibson, I., Leat, P., Hergt, J., Thompson, R., 1991. Chemical and isotopic constraints on the origin of basalts from the Ninetyeast Ridge, Indian Ocean: results from DSDP Legs 22 and 26 and ODP Leg 121. In: Weissel, J., Pierce, J., Taylor, E., Alt, J. (Eds.), *Proceedings of the Ocean Drilling Program, Scientific Results, vol. 121*. Ocean Drilling Program, College Station, TX, pp. 559–590.
- Shipboard Scientific Party in Coffin, M.F., Frey, F.A., Wallace, P.J. et al., 2000. *Proceedings of the Ocean Drilling Program, Initial Reports, 183*. [CD-ROM].
- Tepley, F., Davidson, J., Tilling, R., Arth, J., 2000. Magma mixing, recharge and eruption histories recorded in plagioclase phenocrysts from El Chichón Volcano, Mexico. *Journal of Petrology* 41, 1397–1411.
- VanderAuwera, J., Longhi, J., Duchesne, J., 2000. The effect of pressure on D_{Sr} (plag/melt) and D_{Cr} (opx/melt): implications for anorthosite petrogenesis. *Earth and Planetary Science Letters* 178, 303–314.
- Weis, D., Ingle, S., Damasceno, D., Frey, F.A., Nicolaysen, K., Barling, J., 2001. Origin of continental components in Indian Ocean basalts: evidence from Elan Bank (Kerguelen Plateau, ODP Leg 183, Site 1137). *Geology* 29 (2), 147–150.
- Wallace, G.S., Bergantz, G.W., 2004. Constraints on mingling of crystal populations from off-center zoning profiles: a statistical approach. *American Mineralogist* 89, 64–73.
- Zellmer, G.F., Blake, S., Vance, D., Hawkesworth, C., Turner, S., 1999. Plagioclase residence times at two island arc volcanoes (Kameni Islands, Santorini, and Soufriere, St. Vincent) determined by Sr diffusion systematics. *Contributions to Mineralogy and Petrology* 136, 345–357.